Long Term Performance of Low Cost Motion Sensors

T. Lake*, A.J. Williams, I. Masters
t.lake@swansea.ac.uk

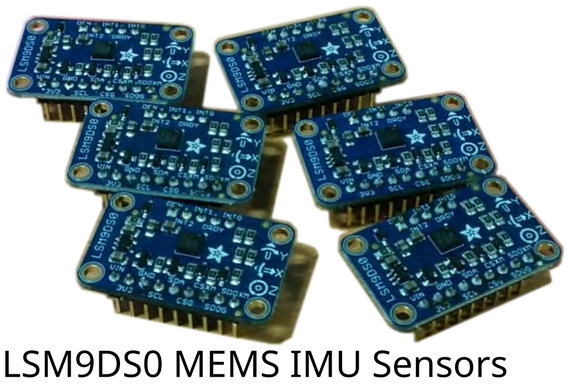

LSM9DS0 MEMS IMU Sensors
The sensor is the chip at the centre of each board, and measures 4mm x 4mm

Microelectromechanical system (MEMS) devices can provide low cost sensors capable of providing a variety of measurements in small packages. A common use is to measure motion using accelerometers, gyroscopes and magnetometers as an inertial measurement unit.

Four LSM9DS0 MEMS IMU sensors (left) were initially deployed on a floating tidal energy device in 2017 and have recorded data over various periods since.

The three plots below show data from the 4 sensors, installed as two pairs (AA & AB in one unit and BA & BB in a second) between April 2019 and April 2020. Long periods without data have been omitted.

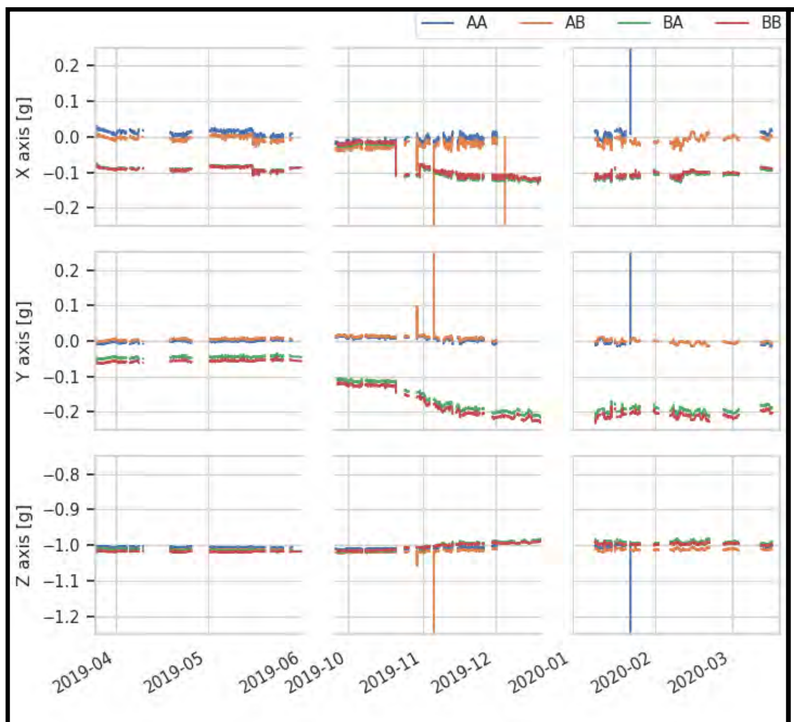

Accelerometer data - 10 minute averages

Initially, all 3 axes on all 4 sensors track each other well, with the exception of an offset between the A and B pairs.

Towards the end of October 2019, the accelerations recorded from the two B sensors (BA, BB) diverge from the two A sensors. This may be due to the unit containing these two sensors moving, which seems more likely than both sensors failing in a consistent and simultaneous manner.

With that exception, there appear to be no notable long term trends in the acceleration data.

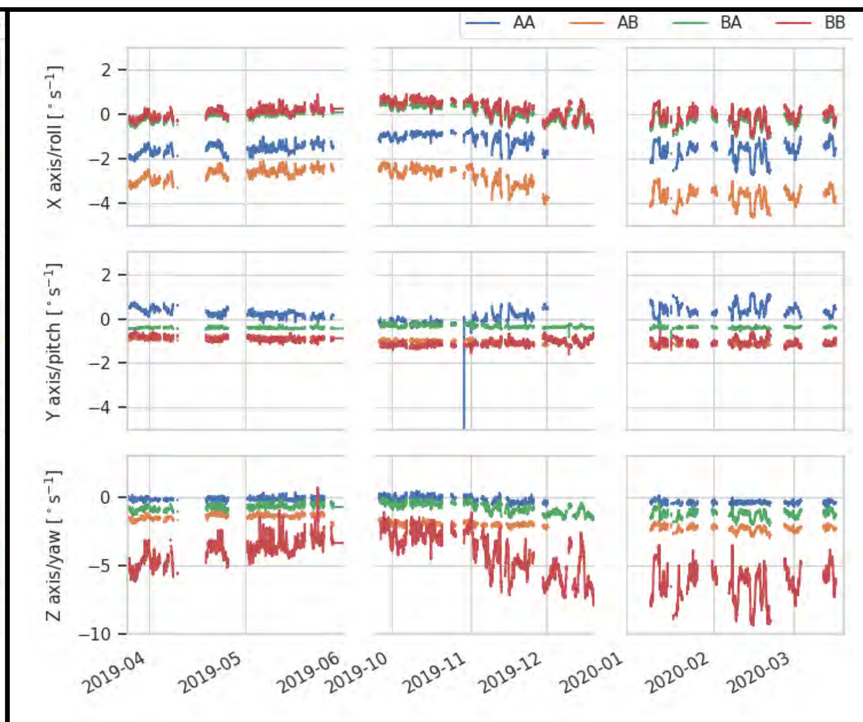

Gyroscope data - 10 minute averages

As with the acceleration data, the four sensors generally track each other well, although the two A sensors appear to be offset from zero by approximately 2 and 3 degrees in roll.

This data has been subject to the least analysis of the three, but the values reported by all four sensors remain consistent over the entire 12 month period shown.

The obvious outlier is the Z/yaw axis on sensor BB, which correlates well with the other three sensors but at an exaggerated scale. As far as can be determined, this is a hardware fault that could be detected by better testing before installation.

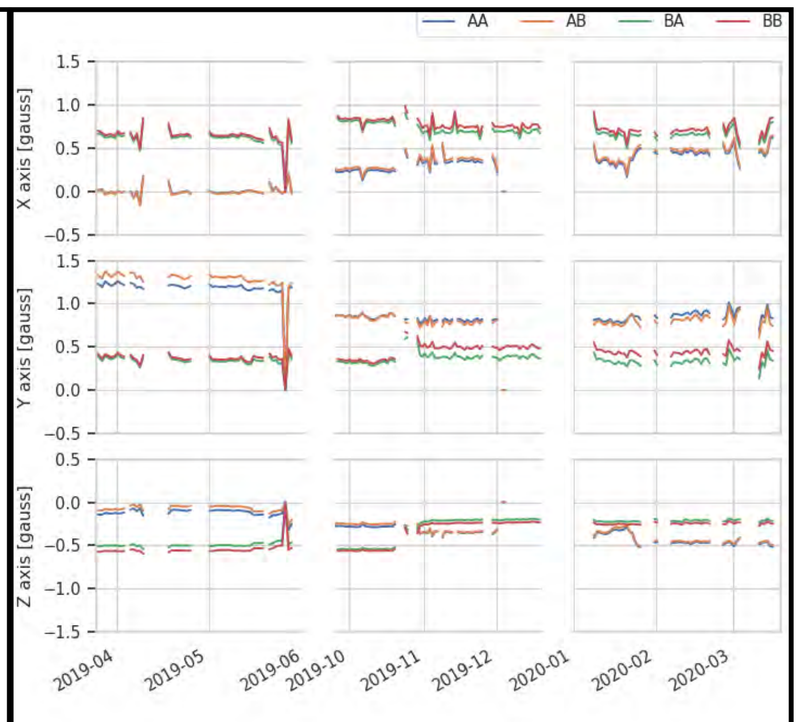

Magnetometer data
24 hour 50 minute averages (tidal day)

Averaged over a tidal day to remove the effects of the platform orienting itself into the tide, the magnetometer data has required the most post-processing to extract the information required.

It can be seen that each pair of sensors has a different mean value for each axis, but consistent in each pair. This reflects the local conditions around each sensor unit. It can also be seen that these mean values have shifted over time - most obvious in October and November 2019 and January 2020 (particularly AA and AB).

The sensors are generally stable, and it would appear that deployments (in a single location) up to one month may be viable without recalibrating. Longer term deployments may need to allow for recalibration periodically on site or, if on a device that rotates as in this case, as a post-process.

General Reliability.

To date, the sensors have been operating for more than 12300 hours across 3 years in a range of environmental conditions. There have been reliability issues since December 2019, when both A unit sensors (AA, AB) began returning data intermittently, and then sensor AA reported invalid acceleration values between January and August 2020.
When last tested, all sensors were still reporting valid data.

Engineering and Physical Sciences Research Council
SUSTAINABLE MARINE ENERGY LTD
EMEC THE EUROPEAN MARINE ENERGY CENTRE LTD
BLACK & VEATCH

COUPLED MODELLING FOR DYNAMIC SUBMARINE POWER CABLES

INTERFACE SENSITIVITY ANALYSIS OF GLOBAL AND LOCAL ENGINEERING MODELS

Rachel Nicholls-Lee, Philipp R. Thies, *Renewable Energy Research Group, University of Exeter*

Introduction: As wind energy moves further offshore, floating platforms are required at deeper depths due to the associated CAPEX and OPEX increase. Subsea cables that transfer the generated power to shore are required to survive and operate reliably in the energetic environment of the open ocean – resulting in the development of dynamic subsea power cables.

Motivation: Fatigue due to cyclic loading from waves and currents is a key concern, and methods are being investigated to assess this through coupled local and global modelling of the turbine/floating platform/mooring/dynamic cable system. The coupled model has many inputs, and the sensitivity of the results to these values is key to the accuracy of the results.

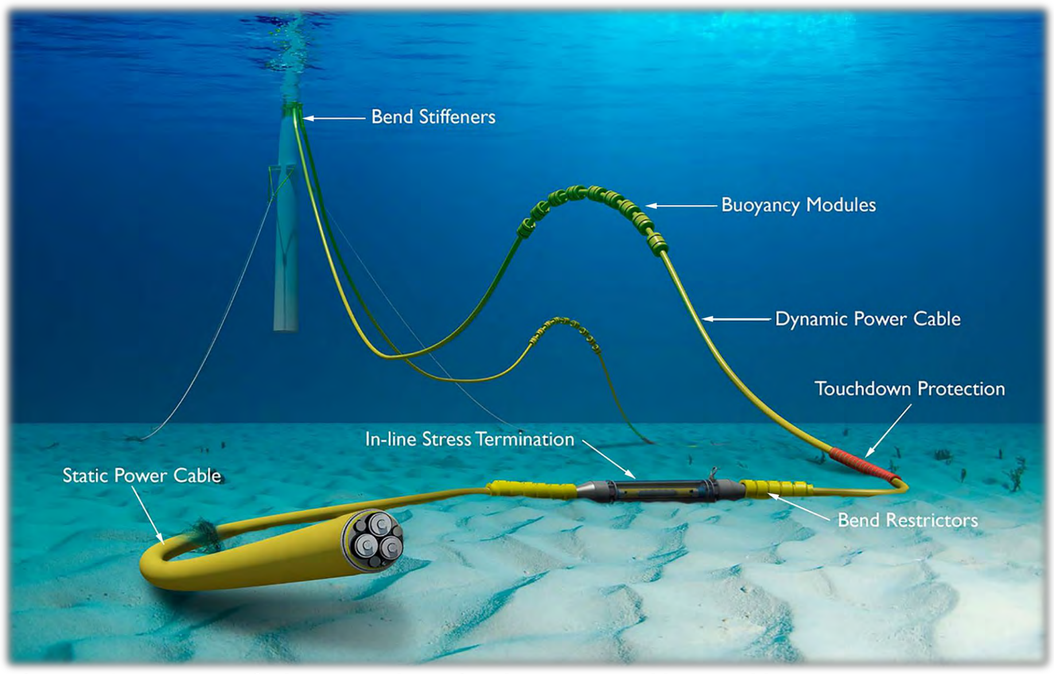

Figure 1: Components of a lazy wave dynamic subsea power cable assembly *(Illustration by Joshua Bauer, NREL)*

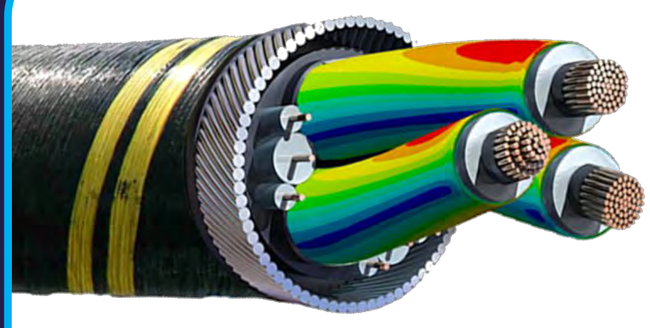

Figure 2: Stress contours on the waterproof Lead Alloy barrier of a subsea power cable from ANSYS [1]

Local Modelling

- Computationally expensive
- Analyse local layerwise structural response of cable
  - Stress, Strain, Deflection
- Calculate overall cable structural properties
  - Bend Stiffness, Axial Stiffness, etc.
- Initial results from Global Analysis inform inputs

Global Modelling

Assess whole system:

- Platform motions in varying sea states, including moorings and dynamic cable (OrcaFlex [2])
- Wind Turbine loads and response (OpenFAST [3])

Requires input of cable local structural properties:

- Bend Stiffness
- Axial Stiffness

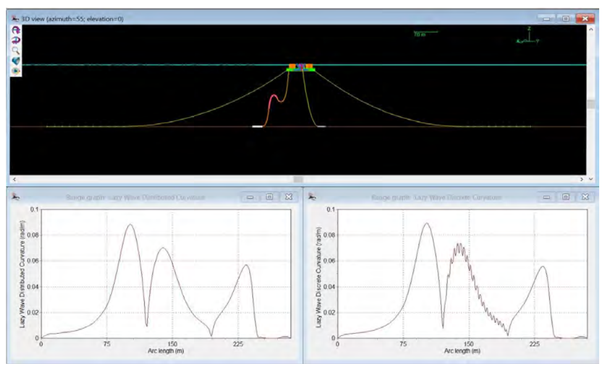

Figure 3: Cable curvature of a lazy wave configuration dynamic subsea power cable with smeared float properties (left) and discrete float properties (right)

Coupled Modelling

Figure 4: NREL 5MW baseline turbine on the OC4 platform

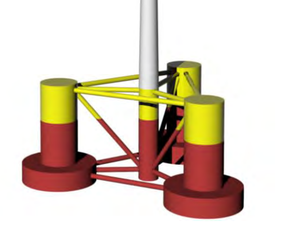

Turbine - NREL 5MW baseline turbine

Platform - DeepCWind OC4 semi-submersible

Cable - Three core, 66kV dynamic subsea cable

Sea state - Representative floating offshore wind farm:

- Most frequent: Hs=1.5m, Tz=4.5s
- Max 1 yr: Hs=8.5m, Tz=10.5s

Local Model – Bend stiffness, axial stiffness

Global Model – Cable curvature, tension

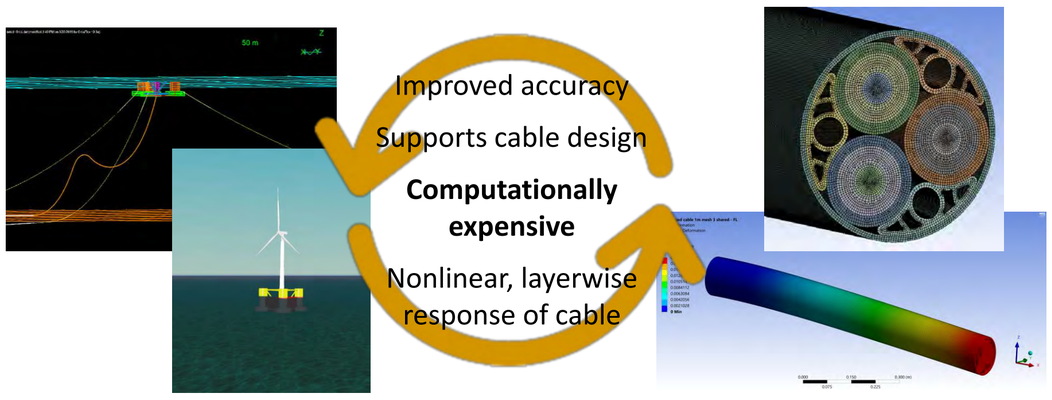

Results

- Run times:
  - **Global Model (16GB RAM)** = 30mins (11mins real time)
  - **Local model (1m, simplified, 128GB RAM)** = 10 hours per single structural stiffness value
- 3.2x Hs, large increase in tension range (TR) (271%) but has little effect on curvature (0.4%)
- 2x axial stiffness, 40%↓ in TR, 1.2%↓ in curvature for **high** bending stiffness
- 2x axial stiffness, 38%↓ in TR, 28%↓ in curvature for **low** bending stiffness
- 7x bending stiffness, 7%↑ in TR, 27%↓ in curvature for **low** axial stiffness
- 7x bending stiffness, 2%↑ in TR, <1%↓ in curvature for **high** axial stiffness

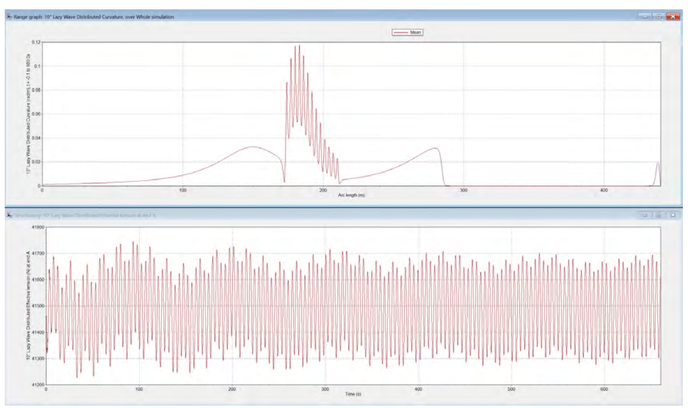

Figure 5: Mean cable curvature of the lazy wave 66kV dynamic subsea power cable with discrete float properties (top) and effective tension in the dynamic cable (bottom) with Hs=1.5m Tz=4.5s

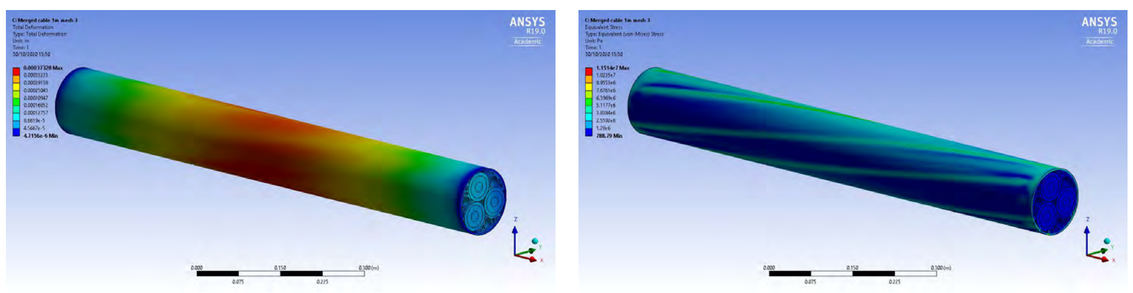

Figure 6: Deflection (left) and stress (right) for a dynamic inter-array power cable determined using ANSYS

Conclusions:

- Local model highly computationally expensive, necessity to ensure inputs and modelling methods are valid and accurate.
- Global model fast for basic runs, useful for initial inputs for local model
- Increasing wave height has little effect on cable curvature
- Cable curvature and tension range more sensitive to axial stiffness changes, especially at low bending stiffness

Future Work:

Investigate sensitivity of coupled model to waves + swell from different directions, cable hysteresis, and friction coefficients between cable layers.

Assess fatigue performance and predict cable life.

Compare to experimental test results.

References:

[1] ANSYS Mechanical 2020 R2, Mechanical's User Guide, ANSYS Inc., 2020

[2] OrcaFlex v11.0f, OrcaFlex Help, https://www.orcina.com/webhelp/OrcaFlex/Default.htm, Orcina Ltd. 2020 (accessed 7th January 2021)

[3] OpenFAST v2.3.0, OpenFAST Documentation, https://openfast.readthedocs.io/en/master/, 2020 (accessed 7th January 2021)

Acknowledgements: This work was supported by the EPSRC Supergen ORE Hub [EP/S000747/1]

R.F.Nicholls-Lee@exeter.ac.uk www.emps.exeter.ac.uk/renewable-energy

Structural performance and fatigue damage assessment for wind turbine blades based on the FSI model

Chizhi Zhang[1], Tarun Choudhary[1], and Michael J Fagan[1]

[1] Department of Engineering, University of Hull, HU6 7RX, UK

Background

- Composite blade is the most vital wind turbine component since its expensive manufacturing cost
- Fatigue is one of the most critical damages of blades due to the cyclic loadings
- Useful models and methods are needed for simulating deteriorating composite blades affected by fatigue damage during lifetime
- FE model and fatigue analysis required for determining remaining useful life and optimum maintenance strategy

Objectives

- To develop a one-way FSI model in finite models for reproducing the performance of composite blades by combining CFD and FEA methods
- To using fatigue analysis model called nCodes for estimating cumulative fatigue propagation and determining fatigue damage during lifetime
- To verify above methods in NREL 5 MW wind turbine blade

Methodology

- Firstly, the FSI model based on the one-way coupling strategy, in which, the aerodynamic load calculated by CFD modelling is imported into FEA modelling as the load boundary condition.

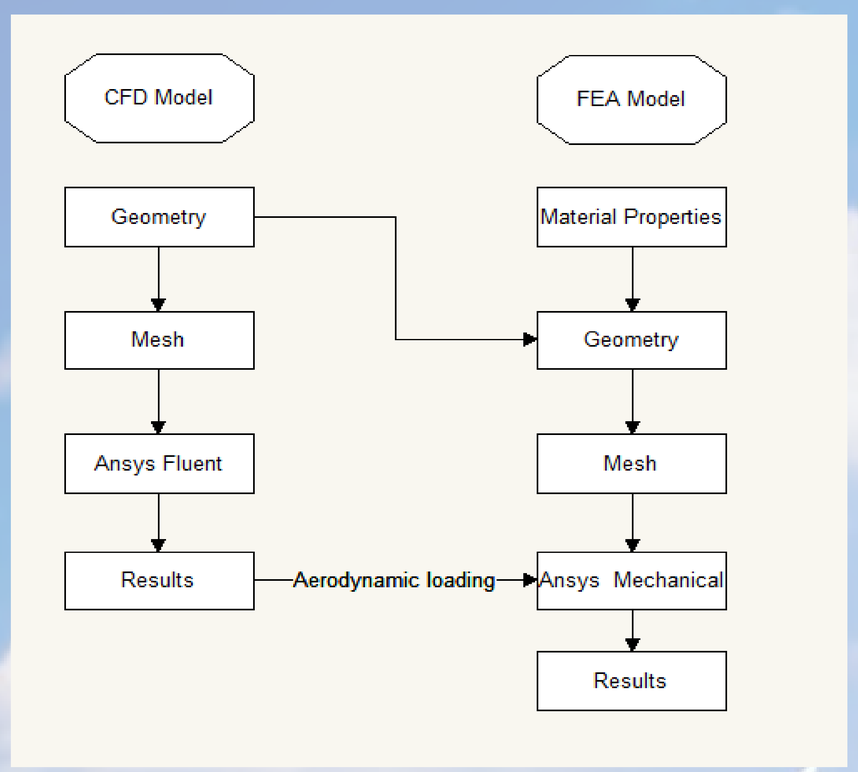

Figure 1 Structure of one-way FSI modelling in flow chart

- Secondly, after inputting material properties and the dynamic wind data from FSI model in the fatigue analysis module, the fatigue damage results can be obtained, and damage hot points can be investigated by nCode module.
- Lastly, a numerical example of NREL 5 MW wind turbine blades was studied to estimate the fatigue damage using FSI model and damage assessment in the offshore environment.

Results

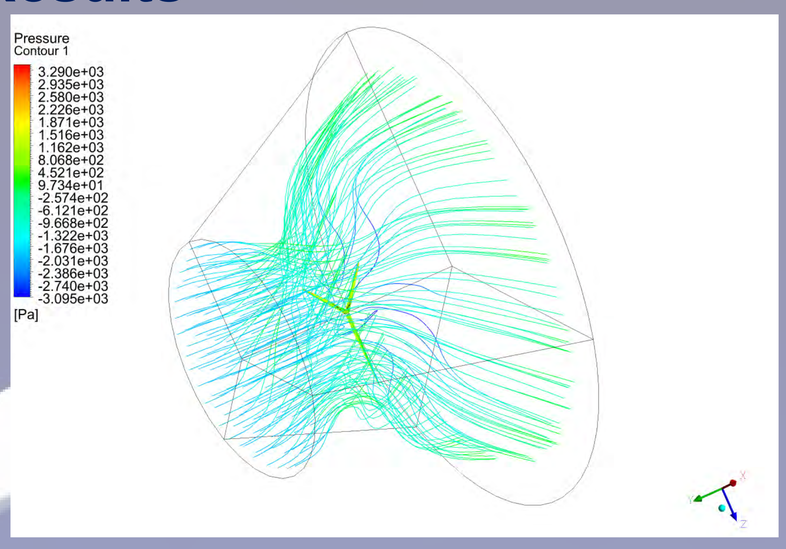

Figure 2 Velocity streamlines crossing the NREL 5MW wind turbine blades in the wind field

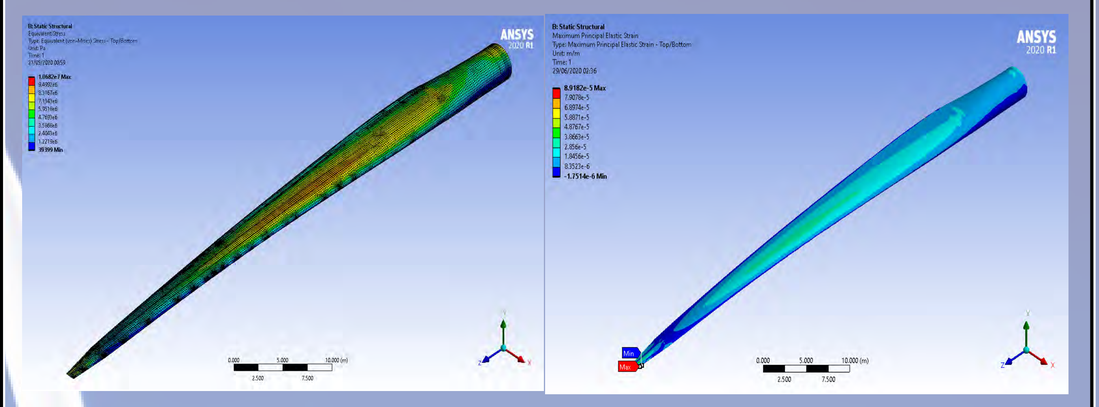

Figure 3 The stress and deformation in FEA after wind pressure

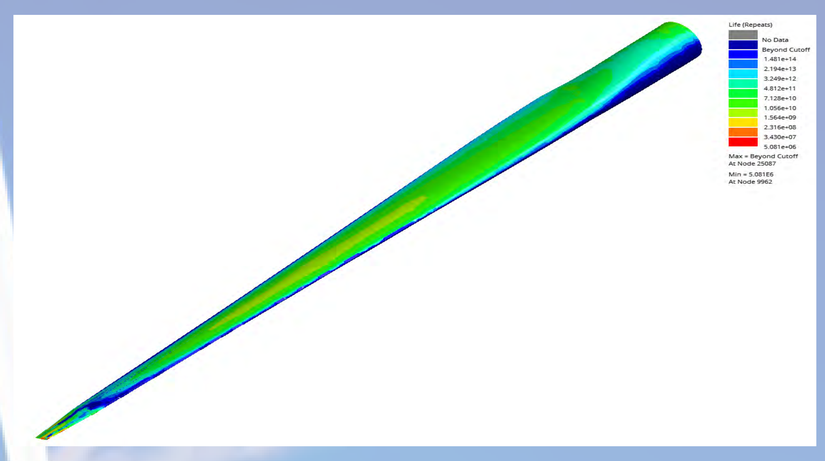

Figure 4 Fatigue life prediction of NREL 5 MW wind turbine blade by nCode

The results show that the critical place for fatigue damage is near the edge of the tip, which is 5.08e6 cycles

Conclusions

This study shows

- ✓ Indicate the pressure of wind turbine blade in various wind speed in CFD module.
- ✓ Investigate the performance of wind turbine blade in FEA static analysis.
- ✓ Predict fatigue damage propagation of composite blades of wind turbines

Future Work

- To improve the more accurate FE model
- Fatigue damage results in work for optimising repair strategy on the composite blades

Acknowledge

- The authors gratefully acknowledge the support of the UK EPSRC through Grant references EP/R004900/1.

Effects of POD Control on Offshore Wind Turbines Structural System

Mohamed Edrah*, Xiaowei Zhao

School of Engineering, University of Warwick, Coventry, CV4 7AL, U.K

*m.edrah@warwick.ac.uk

Background and Motivation

- Increasing penetration of offshore wind power has raised concerns for the GB system operator regarding the dynamic stability of the future system as more conventional synchronous generation will be displaced.
- In securing future system stability, offshore wind turbine (OWTs) are required to provide power oscillation damping (POD) capability.
- Incorporation of POD control on OWTs could induce unfavorable effects on their control and structural systems.

Development of detailed WT model

- Aerodynamics and structural system of the WT are modelled using FAST based on NREL 5-MW offshore WT.
- FAST can be used to exchange data with Simulink introducing great flexibility for electrical system and control implementation.

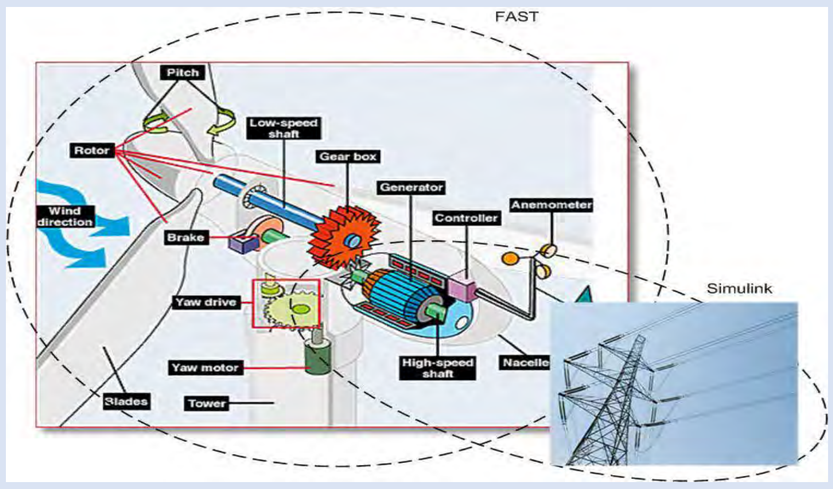

Design and incorporation of POD control

- The proposed POD is based on the conventional lead-lag controller which is the most widely adopted design for industrial applications.
- Active power modulation is used to damp power system oscillations.

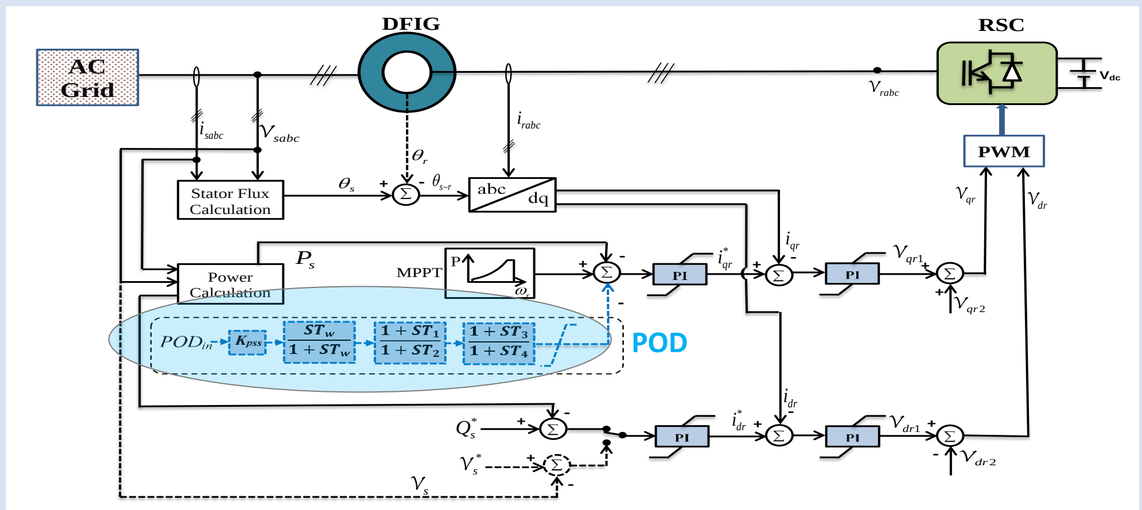

Results

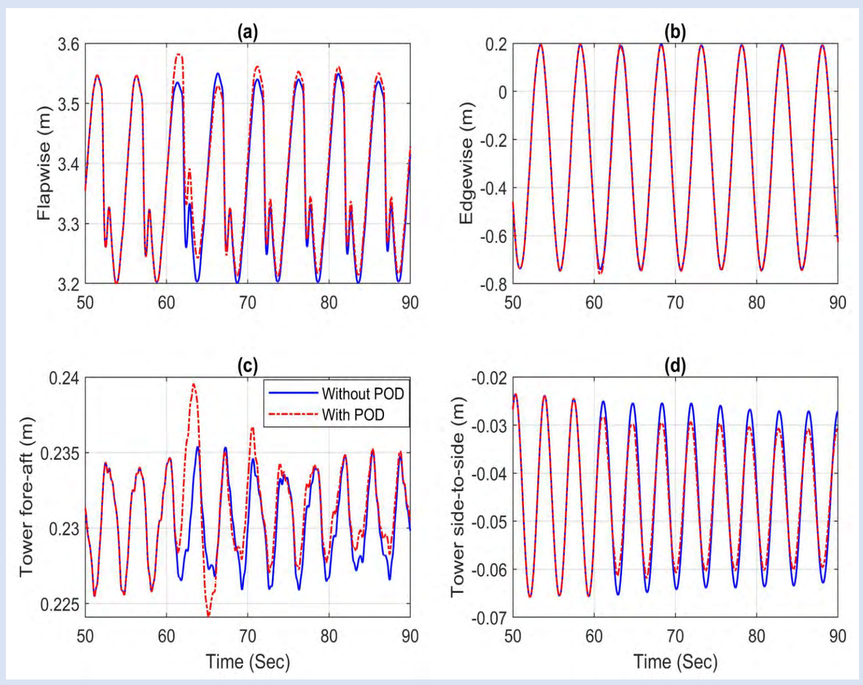

WT blades (a) Flap-wise & (b) Edge-wise tip deflections, and WT tower (c) Fore-aft & (d) Side-to-side displacements.

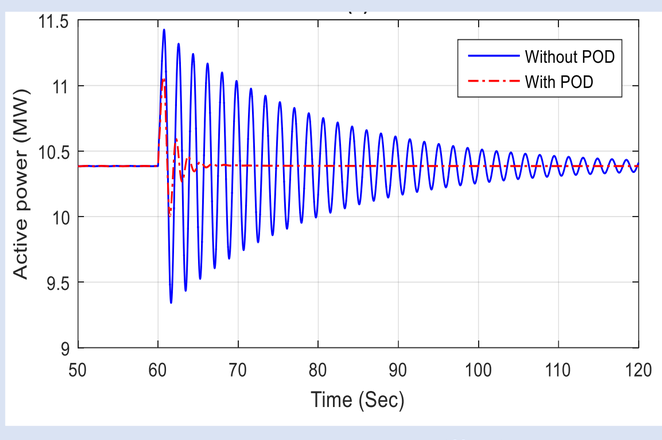

Inter-area power oscillation

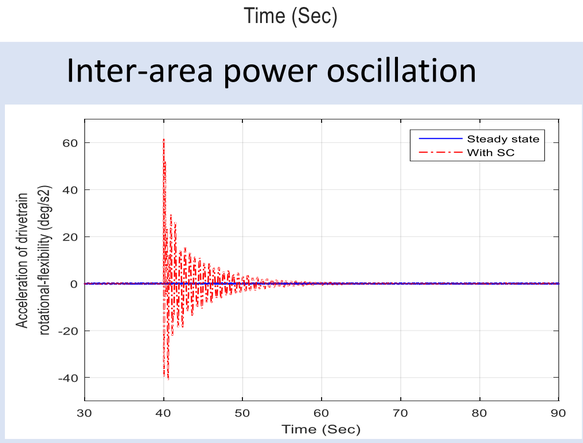

Drivetrain acceleration (grid fault)

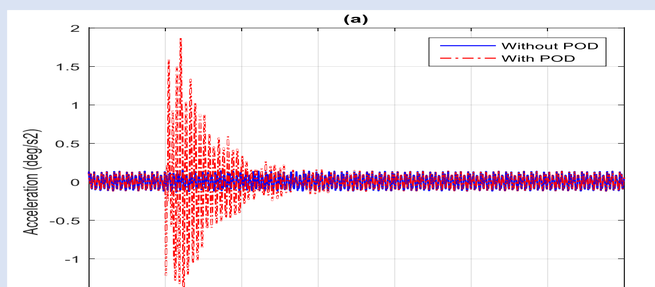

Drivetrain acceleration (POD)

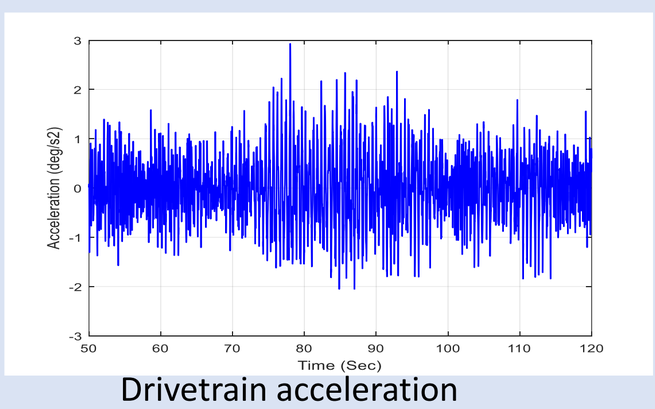

Drivetrain acceleration (variable wind speed)

Conclusions

- POD for OWTs can effectively damp power system oscillations but it can influence WT drivetrain dynamics and hence the blades and the tower.
- The effects of POD on the WT structural system are comparable or less significant as those caused by wind speed variations and grid faults

Future Work

- The effects of other ancillary services such as inertia control on the WT structural system could be investigated.

Component and system reliability in tidal turbine deployments

Stuart Walker[1], Philipp Thies
University of Exeter ([1] Corresponding author: s.walker7@exeter.ac.uk)

Motivation & Aims

Tidal stream energy ➡ The capture of the energy of tidal ebb and flow using devices placed in the tidal stream.
Resource ➡ UK resource potential of 34 TWh per year, potential to supply ~10% of UK electricity.
Predictability ➡ A major advantage. Tidal energy is the only 100% predictable renewable energy source.
Reliability ➡ A current challenge. Low reliability increases cost and limits investment, slowing industry growth.

Though tidal stream energy has the unique advantage of predictability, reliability has limited growth due to perceived risk to investors and high operation and maintenance costs. Reliability is a focus of the TIGER project. To date, there has been no full study of reliability of tidal stream energy industry. This work aimed to:

- Identify and classify the status and performance of all previous deployments of tidal stream energy
- Identify any correlation between failure type and location, device type or design, or other project features
- Study the impact of the diversity of device designs on reliability and reliability growth.

Deployment Types

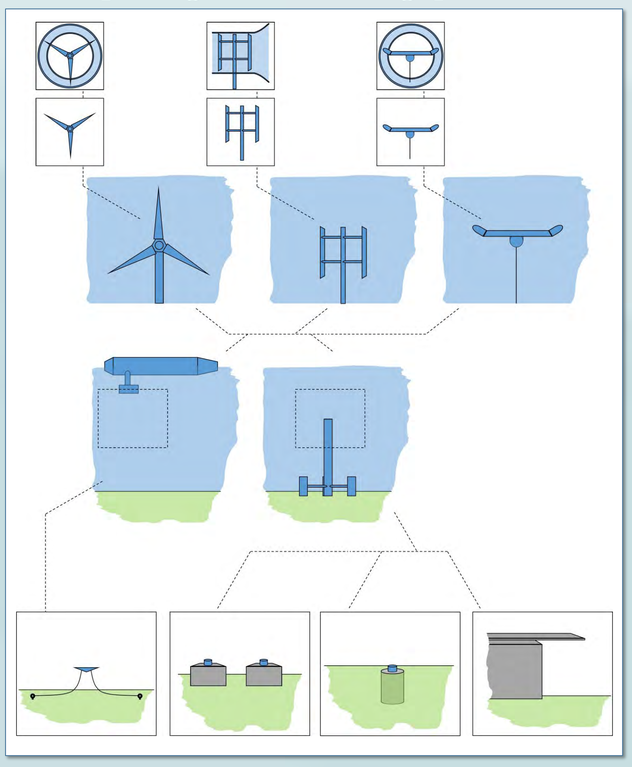

Identified deployments were categorised by:

- Ducting
- Device Type (Horizontal axis, vertical axis, or oscillating)
- Support Structure Type (Fixed or Floating)
- Foundations (Moored, gravity, piled, pontoon structure)
- Grid connection status (none, island grid, mainland grid)
- Number of devices in deployment (1, 2, 3 or more)
- Device power rating (sub-100kW, 100kW to 1MW, over 1MW)
- Site mean and peak flow velocity

Most common:
Single non-ducted 1MW horizontal axis device; fixed structure with gravity base foundations

Deployment Identification

Between 2003 and August 2020, 57 deployments were identified, across 13 countries and all device types.

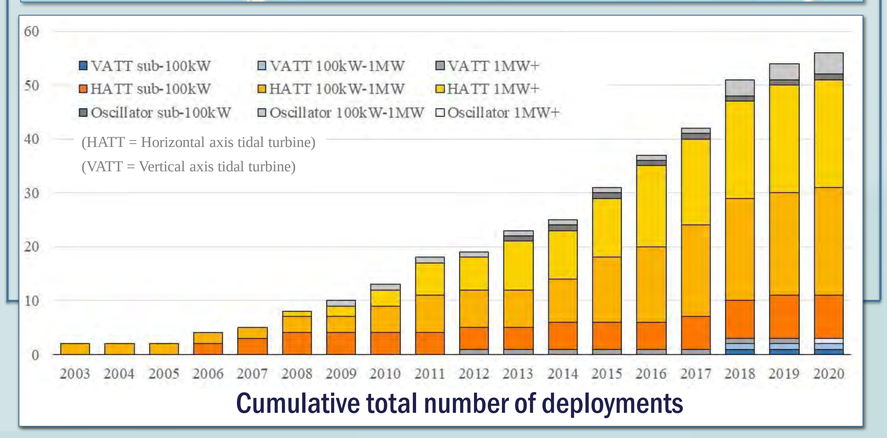

Deployment Status

Performance was measured using availability (A_v):

$$A_v = T_{gen} / T_{in\text{-}limits}$$

For deployment duration T:
T_{gen} = Time device generated power
$T_{in\text{-}limits}$ = Time with flow velocity within device generation range

Deployments were classified as:

Successful:	Planned duration	✔	Planned availability	✔
Underperformed:	Planned duration	✔	Planned availability	✖
Curtailed:	Planned duration	✖	Planned availability	
Failed:	Failure of device or equipment			

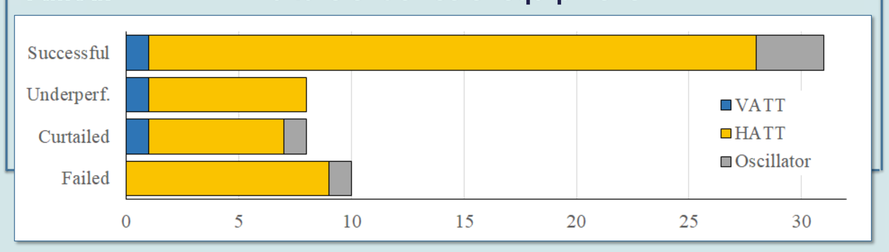

Results

- Of the 10 total failures (17% of deployments), four were blade failures, three were generator failures, and three were failures of monitoring equipment, meaning that deployments were unable to meet their license conditions.
- Of the 8 total curtailments (14% of deployments), five were curtailed due to low performance, and three were curtailed to avoid failure caused by fatigue.

Notable relationships:

- **Foundation type:** Floating foundations = less failures vs. fixed foundations
  Though more curtailments, suggesting floating devices tend to be removed before failure
- **Ducting:** More failures vs. non-ducted devices
- **Learning:** More failures were seen earlier in the 2003-2020 window
- **Flow rate:** Sites with high mean and peak flow rates experienced more failures

Tidal stream energy is a young industry, with 1.4 million operating hours accumulated since 2003.

- 86% of these hours were achieved by horizontal axis devices.
- Current failure rates are around 0.065 major failures per turbine per year, similar to that of onshore wind energy after the same duration of deployment.

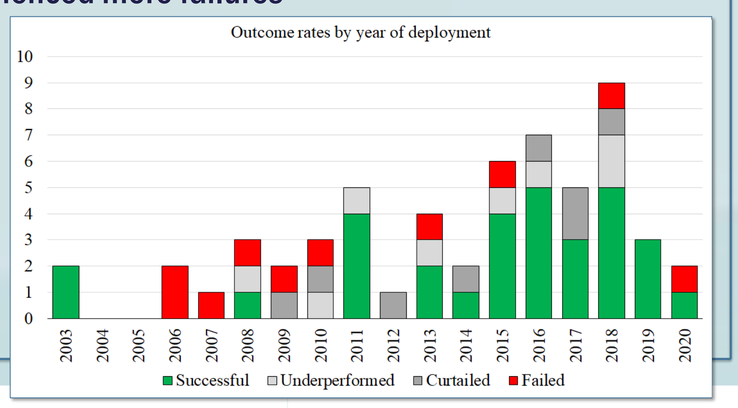

Conclusions

- Learning rate describes the fraction of cost reduction per doubling of installed capacity. Data collected in this study suggests a learning rate of 10.9% for tidal stream energy. This is comparable to other renewable energy technologies.
- Tidal stream energy device reliability is improving through learning, particularly in horizontal axis devices, which have accumulated the vast majority of total operating hours.
- This learning improves reliability, reduces cost of energy and improves investor outlook.

10.9%
Learning rate

EUROPEAN UNION
Interreg France (Channel Manche) England
European Regional Development Fund
TIGER TIDAL STREAM INDUSTRY ENERGISER
UNIVERSITY OF EXETER

Walker, S., Thies, P., *A review of component and system reliability in tidal turbine deployments,* Renewable and Sustainable Energy Reviews (in press)

Extreme Responses of a Raft Type Wave Energy Converter

Tom Tosdevin*[1], Siya Jin[1], Andrea Caio[2], Dave Simmonds[1], Martyn Hann[1], Deborah Greaves[1]

1 University of Plymouth, Plymouth, United Kingdom
2 Mocean energy ltd, Edinburgh, United Kingdom
*Corresponding email: tom.tosdevin@postgrad.plymouth.ac.uk

Introduction

This work investigates the extreme mooring loads of a raft type wave energy convertor (WEC) using long irregular wave time series to estimate the extreme value distribution (EVD) of the design sea state for a 3 hour exposure time. The ability of embedded focus waves to support the EVD estimate and produce loads at it's upper percentiles is then explored using;

- The conditional random response wave (CRRW) method
- The constrained NewWave (CNW) method

Embedded focus waves

- The NewWave method produces the average profile of the extreme wave scaled to a particular percentile of the EVD of the wave amplitude.
- Hann *etal* [1] constrained NewWaves in random backgrounds to study the extreme mooring loads of a taught moored, bottom referenced point absorber WEC. The natural progression would be to study the effect of constraining response conditioned focus waves into random backgrounds which is the focus of this work.
- The CRRW method developed in Dietz [2] results in a response conditioned wave profile constrained into a random irregular background. The constrained profile is the wave predicted to produce the extreme mooring loads of the device according to its response amplitude operators (RAOs).

Device and experimental set up

- A 1:20 scale model of Mocean Energy's Blue Star WEC was used to study the extreme mooring loads (Fig.1).
- Blue Star is a two body raft type WEC which on this occasion was moored using a 'Lazy S' arrangement (Fig. 2).
- The model did not contain any power take off (PTO) in line with the envisaged survival strategy that involves switching off the PTO (i.e. free hinge).

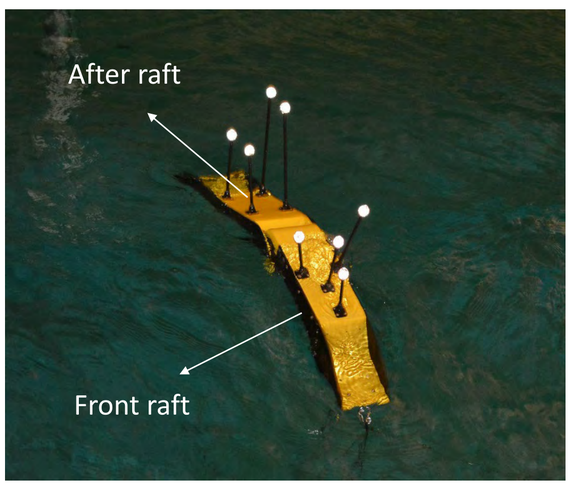

Fig.1 Blue Star WEC.

Fig.2 Lazy S mooring.

Methods

- The 1 year return contour (Hs, Tp) of the EMEC site was searched to determine the design sea state.
- The full scale equivalent of 18 hours of irregular waves were run for the design sea state to predict the EVD for the mooring loads using a peak over threshold method with the threshold at the 90th percentile.
- 20 CRRW and 30 CNW profiles were used to try and produce mooring loads at the higher end of the EVD, 52 seconds of random irregular waves were simulated before the occurrence of the extreme.
- The CRRW and CNW profiles are compared to the waves producing the 6 largest responses from the 18 hours of irregular wave data.

Results

- The Observed profiles from the irregular wave runs which led to the 6 largest mooring loads were found to be more similar to CNWs than CRRWs (Fig.3, Fig.4).
- The CRRWs, shown by black vertical dashed lines (Fig.5), did not produce mooring loads at the higher end of the EVD.
- The CNWs, shown by red vertical dashed lines (Fig.5), produced mooring loads at the higher end of the EVD, Larger than those produced by the CRRW or long irregular waves shown by green vertical dashed lines (Fig.5).

Discussion

The average profile leading to extreme mooring loads more closely matched the CNWs (Fig.3, Fig.4) in the design sea state due to the occurrence of rare snatch loading events. These occurred when the Lazy S mooring became taught which caused an abrupt change in device behavior meaning that the RAOs on which the CRRW profiles are based became unsuitable. For other sea states tested, not shown here, where no snatch loading occurred the CRRWs produced larger mooring loads than the CNWs.

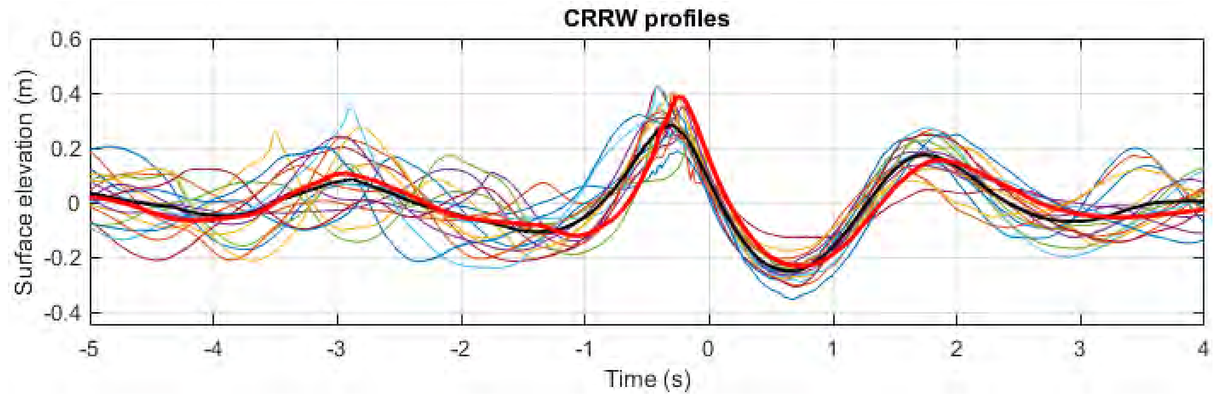

Fig.3 Thirty experimentally measured CRRW profiles with the average shown in black. The average of the observed profiles leading to the 6 largest mooring loads from the 18 hours of irregular waves is shown in red.

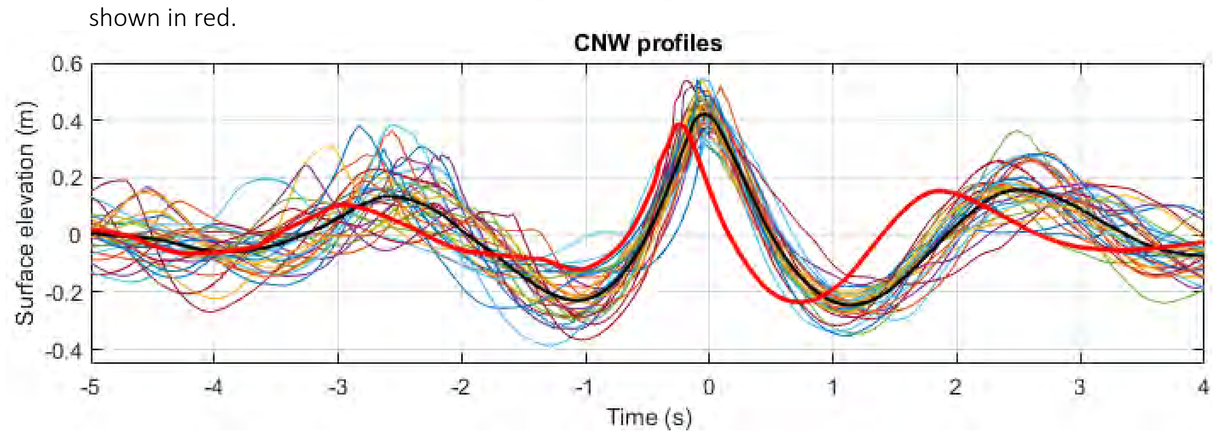

Fig.4 Twenty experimentally measured CNW profiles with the average shown in black. The average of the observed profiles leading to the 6 largest mooring loads from the 18 hours of irregular waves is shown in red.

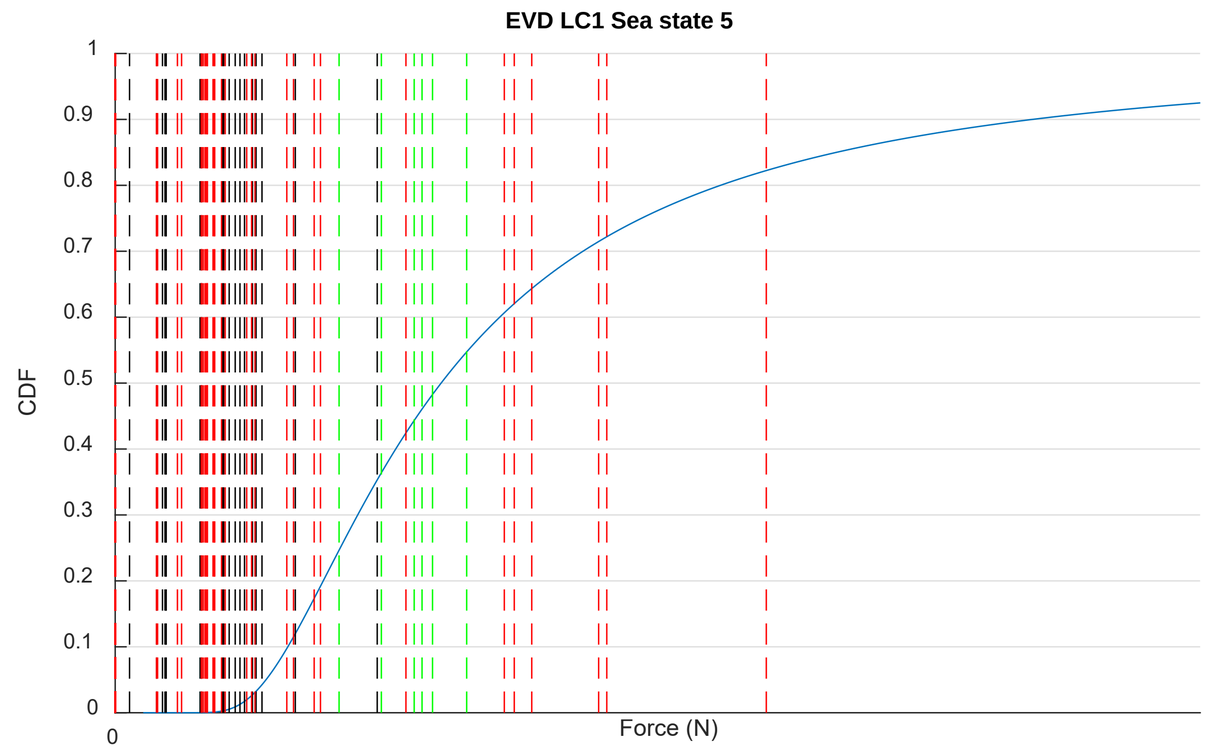

Fig.5 EVD (blue) with maximum mooring load responses of 30 CNWs (black), 20 CNWs (red) and the 6 largest mooring loads from the 18 hours of irregular waves (green) overlaid. Force magnitudes have been obscured by removing the x axis values.

Few higher percentile mooring loads were observed, this suggests that the predicted EVD should be reconsidered. It is likely that the snatch loads change the shape of the distribution above a threshold and so combining multiple distributions may be a more suitable approach [3,4] than the one used here. This will be considered along with further results in a conference paper for EWTEC 2021 hosted at the University of Plymouth.

Conclusions

- Extreme responses in sea states in which snatch loading occurred were more successfully reproduced by CNWs than CRRWs in this instance.
- This result serves as a reminder that response conditioned methods are only appropriate when the behavior of the device or mooring is unchanging over the range of possible wave sequences for the sea state.

References

[1] M. Hann, D. Greaves, A. Raby, and B. Howey, "Use of constrained focused waves to measure extreme loading of a taut moored floating wave energy converter," Ocean Engineering, vol. *148*, pp.33-42, 2018.
[2] Dietz, J.S., 2005. *Application of conditional waves as critical wave episodes for extreme loads on marine structures*. Technical University of Denmark (DTU).
[3] Hsu, W.T., Thiagarajan, K.P. and Manuel, L., 2017. Extreme mooring tensions due to snap loads on a floating offshore wind turbine system. *Marine Structures*, *55*, pp.182-199.
[4] Song, X., Wang, S., Hu, Z. and Li, H., 2019. A hybrid Rayleigh and Weibull distribution model for the short-term motion response prediction of moored floating structures. *Ocean Engineering*, *182*, pp.126-136.

Model-Free Semi-Active Structural Control of Floating Wind Turbines

Dr Hongyang Dong and Prof Xiaowei Zhao

School of Engineering,

University of Warwick, Coventry, UK

Abstract

This study addresses the load/vibration reduction problem of floating wind turbines (FWTs). Based on the tuned mass damper (TMD), a novel semi-active structural control method is designed to mitigate the floating platform's vibration. Different from existing results, the proposed control method is model-free and insensitive to system uncertainties and unmodelled dynamics. We base our design on the model-free adaptive control (MFAC) method [1]. A data-driven surrogate model is established to approximate the unknown nonlinear system through the dynamic linearization technique. Then a quadratic programming module is embedded in our MFAC-based semi-active structural controller for constraint handling and control allocation purposes. High-fidelity simulation results show that the proposed model-free semi-active controller can address the limitations of existing results and significantly reduce the platform's vibration.

Methodology

Objective: Reducing the load/vibration caused by wave and wind via a semi-active tuned mass damper (TMD) for the FWT.

Main methods: Model-free adaptive control, quadratic programming.

Control input: Spring's stiffness (k) and damper's coefficient (c).

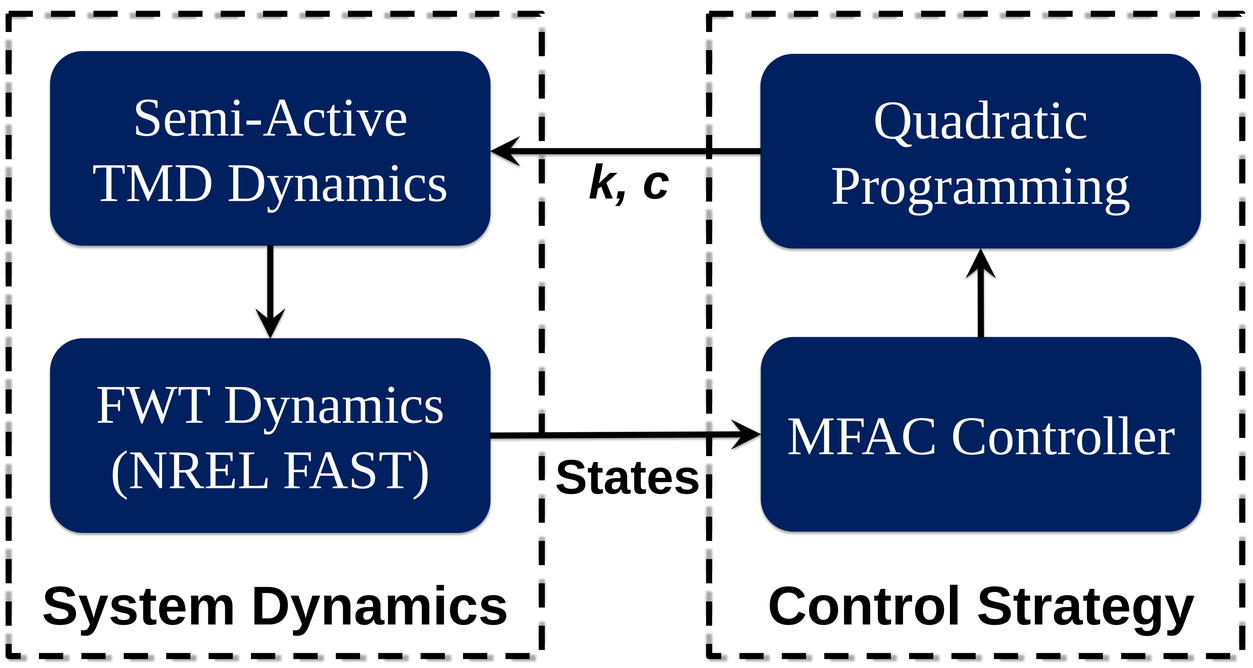

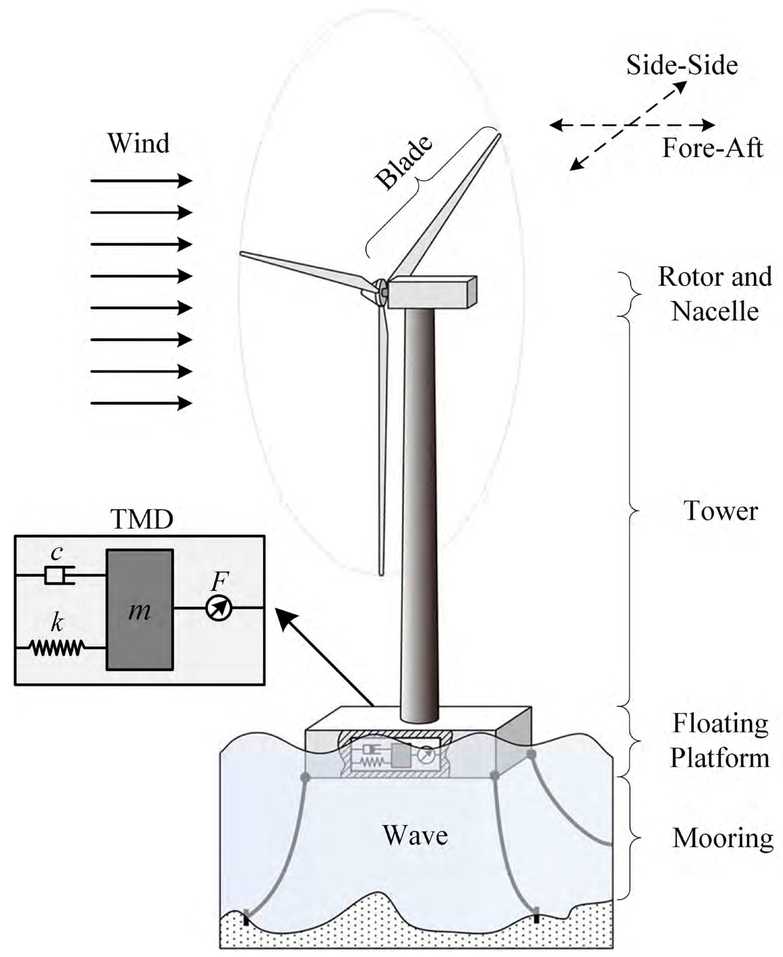

Fig. 1 A floating wind turbine on a barge platform with a fore-aft TMD (adapt from [2]).

Simulations and Discussions

1) Our method is model-free and semi-active, addressing the limitations of existing results.
2) We carried out high-fidelity simulations with the NREL FAST.
3) Simulation results show that our method has better performance than passive TMD methods.
4) Our semi-active control method also leads to a comparable performance with the H-infinity based active structural controller [2].

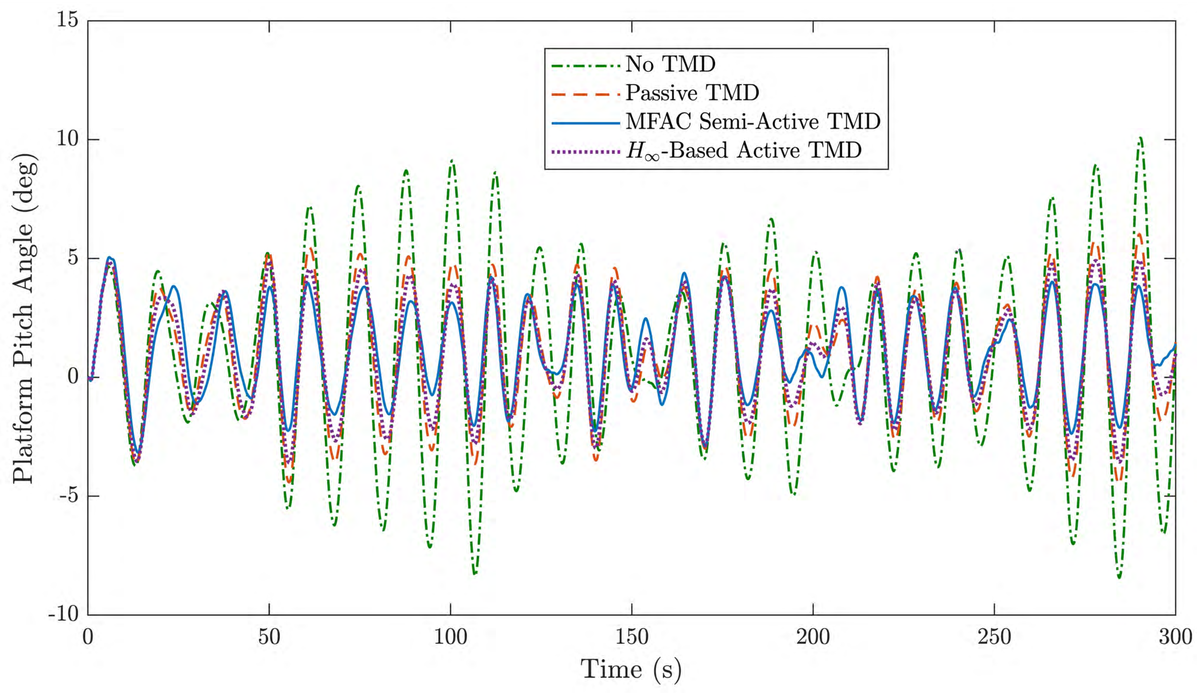

Fig. 2 Simulation results of the platform pitch angles

Reference

1. Z. Hou and S. Jin, "A novel data-driven control approach for a class of discrete-time nonlinear systems," IEEE Transactions on Control Systems Technology, vol. 19, no. 6, pp. 1549–1558, 2011.
2. X. Li and H. Gao, "Load mitigation for a floating wind turbine via generalized H∞ structural control," IEEE Transactions on Industrial Electronics, vol. 63, no. 1, pp. 332–342, 2016.

How relative submergence changes the wake recovery behind tidal stream turbines

Pablo Ouro

pablo.ouro@manchester.ac.uk

Department of Mechanical, Aeronautical and Civil Engineering, University of Manchester, UK.

3rd Annual Assembly
Supergen ORE Hub

Motivation

At every tidal site the local environmental conditions related to water depth or bathymetry distribution are different. These notably impact the flow dynamics, e.g. velocity profile distribution or bed-generated turbulence production, thus directly affecting the energy generation capabilities of tidal stream turbine arrays. Hence, there is a need to individually investigate the array layout that maximises the energy generation at any site.

Relatively low submergences, i.e. when turbines occupy a large proportion of the water column, can have an immediate effect in the turbine wake dynamics, restricting its expansion and thus diminishing the recovery rate. Consequently, as this reduces the energy generation capabilities from secondary rows, it is necessary to identify and quantify the changes in the wake recovery mechanism that depend on the relative water depth.

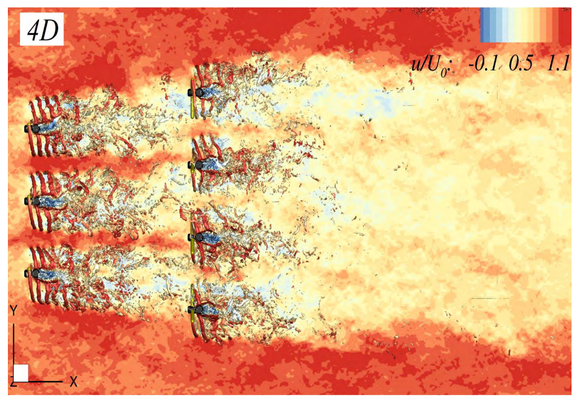

Figure 1. Array of seven tidal turbines simulated using DOFAS [4].

Digital Offshore Farms Simulator

DOFAS (Digital Offshore FArms Simulator) is a state-of-the-art in-house code that adopts the method of Large-Eddy Simulation (LES) [1,2,4] to resolve the large-scale turbulent flow structures, highly present in tidal turbines hydrodynamics, while the small scales are modelled with the WALE sub-grid scale model. DOFAS was validated [4] in the prediction of the hydrodynamics and structural loads in prototype tidal farms [3].

DOFAS adopts the fractional-step method with a Runge-Kutta predictor is to approximate convection and diffusion terms. The fluid domain is discretised with a Cartesian mesh using central differences to compute velocity fluxes. DOFAS is fully parallelised with MPI and features an immersed boundary method to represent solid bodies, an actuator line model to simulate turbine rotors, a synthetic eddy method to generate artificial inflow turbulence.

Why does water depth play a key role in the wake recovery dynamics?

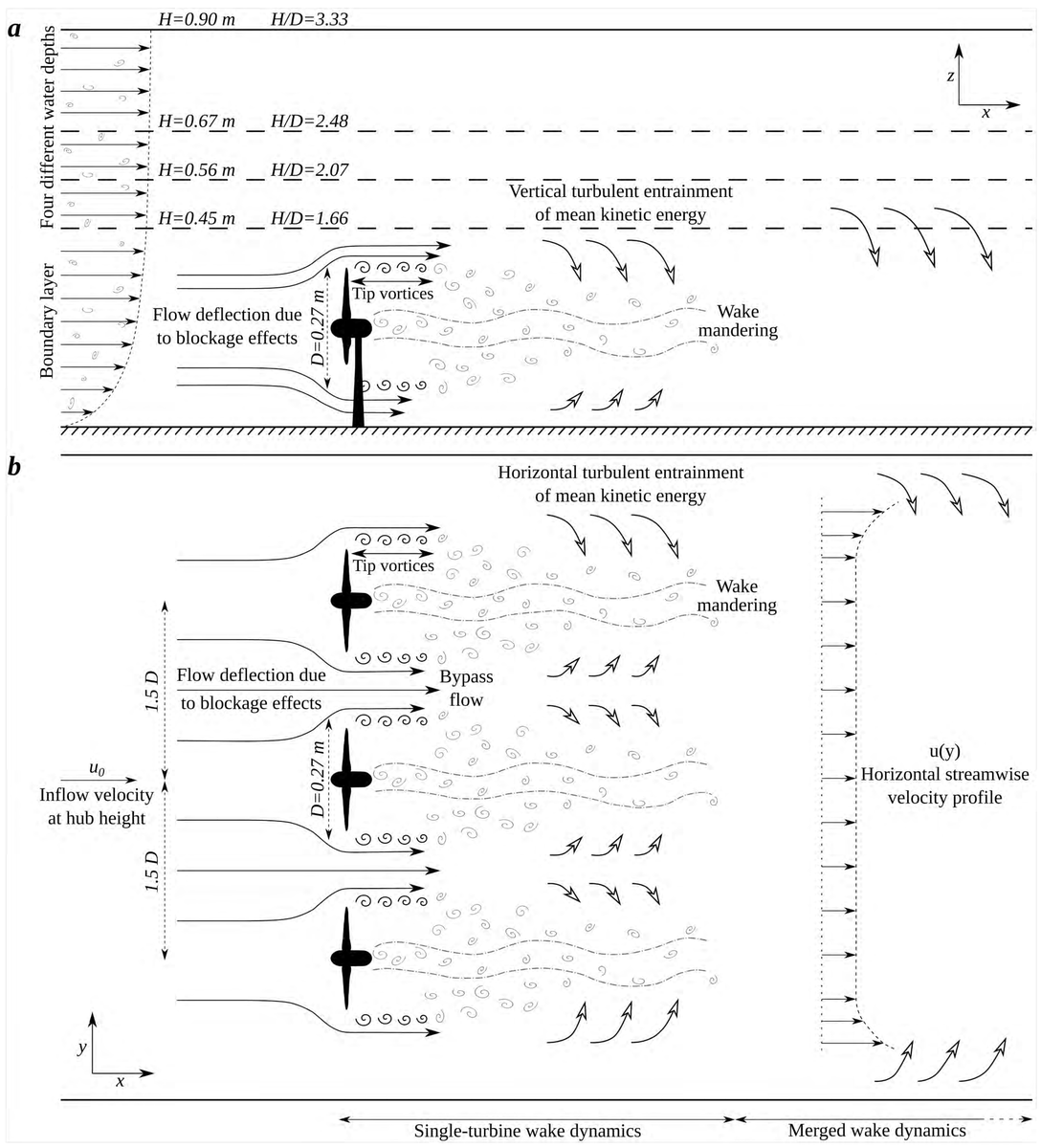

Tidal stream turbine array layouts have to be designed to efficiently harness energy under various operating conditions. The operation of tidal turbines differs from wind turbines because of their proximity to two vertical bounding layers, i.e. bottom bed and free-surface. Identifying the physical mechanisms involved in the wake recovery and their contribution under different environmental conditions, in particular at different water depths, is key to designing efficient arrays.

For this, we analysed the terms in the transport equation for mean kinetic energy (MKE) (Eq.1). Based on previous research in wind farms [5], we are particularly interested in understanding the role of the transport terms in replenishing MKE over the wake region. Figure 2 depicts the flow dynamics involved in the recovery of tidal turbine wakes, outlining the turbulent transport of MKE over the horizontal and vertical directions. The latter has proven to be responsible for the energy generation in large wind farms [5] but its relevance in tidal farms has not been quantified.

Convective transport of MKE | Transport due to pressure | Transport due to viscous stresses | Viscous dissipation

$$\langle u_j \rangle \frac{\partial \langle u_j \rangle^2/2}{\partial x_j} = -\langle u_j \rangle \frac{1}{\rho}\frac{\partial \langle p \rangle}{\partial x_i} + \frac{\partial}{\partial x_j}\left[\upsilon \frac{\partial \langle u_j \rangle^2/2}{\partial x_j}\right] - \upsilon \frac{\partial^2 \langle u_j \rangle^2/2}{\partial {x_j}^2}$$

$$- \frac{\partial}{\partial x_j}\langle u_j \rangle \langle u_i' u_j' \rangle + \langle u_i' u_j' \rangle \frac{\partial \langle u_j \rangle}{\partial x_j} + \frac{1}{\rho}\langle u_i \rangle f_i$$

Transport due to shear stresses | Turbulent dissipation (production of tke) | Power extracted by turbines

Figure 2. Schematic of (a) the wake recovery behind a tidal turbine for different submergence rates and flow phenomena involved in the vertical transport of MKE. and (b) the wake recovery behind a row of tidal turbines and key flow structures involved in the horizontal transport of MKE.

Turbulent transport of mean kinetic energy

Figure 3 presents the profiles of turbulence-driven MKE fluxes averaged over *10D* behind the turbine. In Fig. 3a, positive values indicate downwards flux, and vice-versa, while in Fig. 3b, positive values indicate MKE transfer towards negative *y*-direction (into the wake region), and vice-versa. Larger water depths increase the amount of MKE available above the turbine and leads to greater vertical transport of MKE (Fig. 3a) whilst weaker horizontal transport of MKE (Fig. 3b).

Our LES results show that under relatively shallow conditions, the vertical expansion of the wake is constrained when in close proximity to free-surface layer. The spread of turbulent momentum exchange across the water depth is also constrained by the free-surface presence, as observed from vertical Reynolds shear stresses. The intensity of these stresses decreases at a faster rate for the shallower conditions. Conversely, levels of horizontal Reynolds shear stresses are greater for shallower flows.

Our research suggests that turbine rows in large arrays could be deployed more closely together for ratios of water depth to turbine diameter (H/D) approximately over 2.

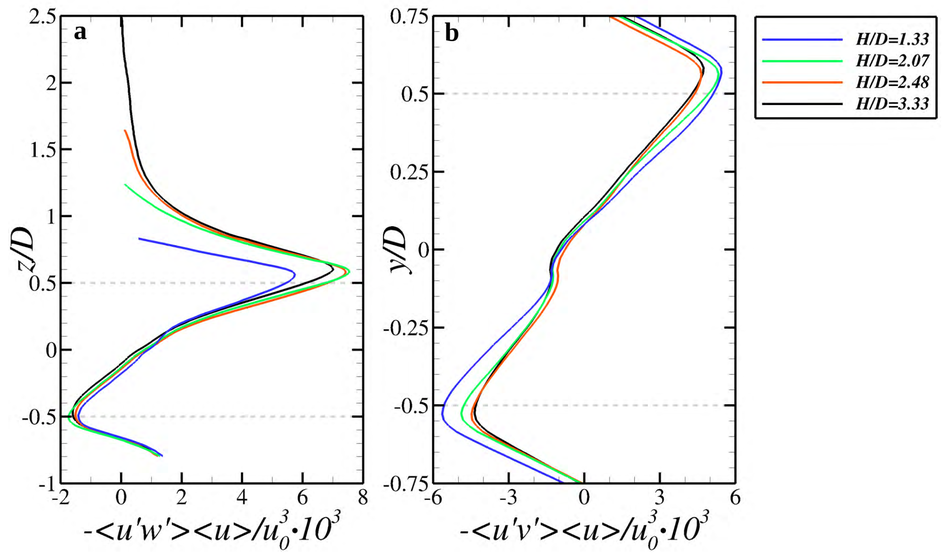

Figure 3. Vertical (a) and horizontal (b) fluxes of MKE averaged over the streamwise direction behind the middle turbine in a three in-line array.

References

[1] **P. Ouro**, T. Stoesser. 2019. Impact of Environmental Turbulence on the Performance and Loadings of a Tidal Stream Turbine. *Flow, Turbulence and Combustion*. 102: 613-639.
[2] **P. Ouro**, M. Harrold, T. Stoesser, P. Bromley. 2017. Hydrodynamic performance and structural assessment of a horizontal axis tidal turbine prototype. *Journal of Fluids and Structures. 71: 78-95.*
[3] T. Stallard, R Collins, R Feng, J Whelan. 2013. Interactions between tidal turbine wakes: experimental study of a group of three-bladed rotors. *Phil Trans R Soc A.* 371: 20120159.
[4] **P. Ouro**, L. Ramirez, M. Harrold. 2019. Analysis of array spacing on tidal stream turbine farm performance using Large-Eddy Simulation. *J Fluids Struct*. 91: 102732.
[5] Cal B, Lebron J, Castillo L, Kang H, Meneveau C. 2010. Experimental study of the horizontally averaged flow structure in a model wind-turbine array boundary layer. *J Renew Sust Energy*. 2: 013106.

Progress on the design of a novel wave energy converter based on hydrodynamic lift forces (LiftWEC)

Dr Abel Arredondo-Galeana[a], Dr Weichao Shi[a] , Dr Matt Folley[b], Prof Feargal Brennan[a]

[a] *Department of Naval Architecture, Ocean & Marine Engineering, University of Strathclyde*

[b] *School of Natural and Built Environment, Queen's University Belfast*

Motivation

The hydrodynamics and structural requirements of most of types of wave energy converters (WECs) are unique and analogies in other industries are difficult to find (Schmitt, 2012). One exception to this are wave bladed cyclorotors, which are devices that utilise foils to generate lift. Foils and lift are utilised in a wide variety of devices for energy extraction (wind turbines, tidal turbines, helicopters, propellers) hence knowledge of these fields is transferable to wave bladed cyclorotors. In such devices, the hydrofoils are driven by the orbital particle motion under a wave (Figure 1). The phase of the rotation is out of phase to that of the incoming wave to generate lift on the hydrofoils.

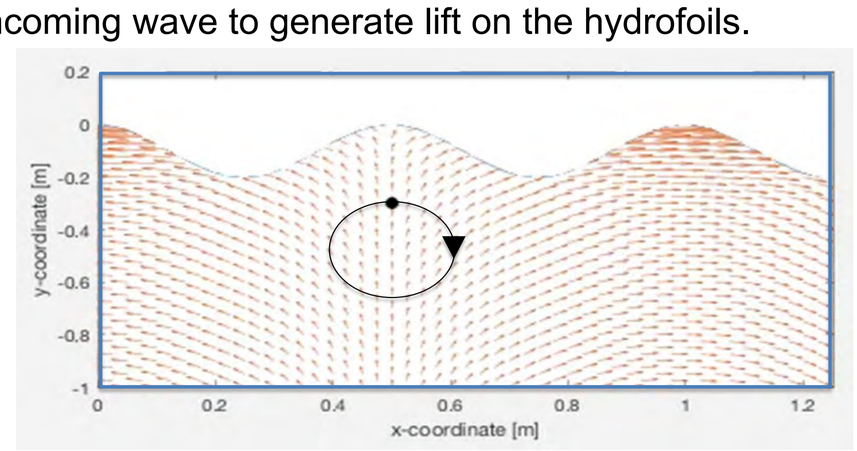

Figure 1. Orbital particle motion and varying velocity field under wave

LiftWEC: a wave bladed cyclorotor

Here we introduce LiftWEC: a wave bladed cyclorotor. A typical configuration of the rotor under a wave crest is shown in figure 2. The device consists of two hydrofoils joined to a central shaft by lateral spokes. The support structure is a frame that holds the central shaft in place through a couple of bearings. Assuming regular waves, the rotation of the hydrofoils is driven by the wave orbital motion, and so the rotational frequency of the rotor is the same as that of the incoming wave. The rotational phase, however, is controlled initially so hydrofoil 1 operates at a 90 degrees phase with respect to that of the wave velocity (v). This phase difference generates the lift in the hydrofoils.

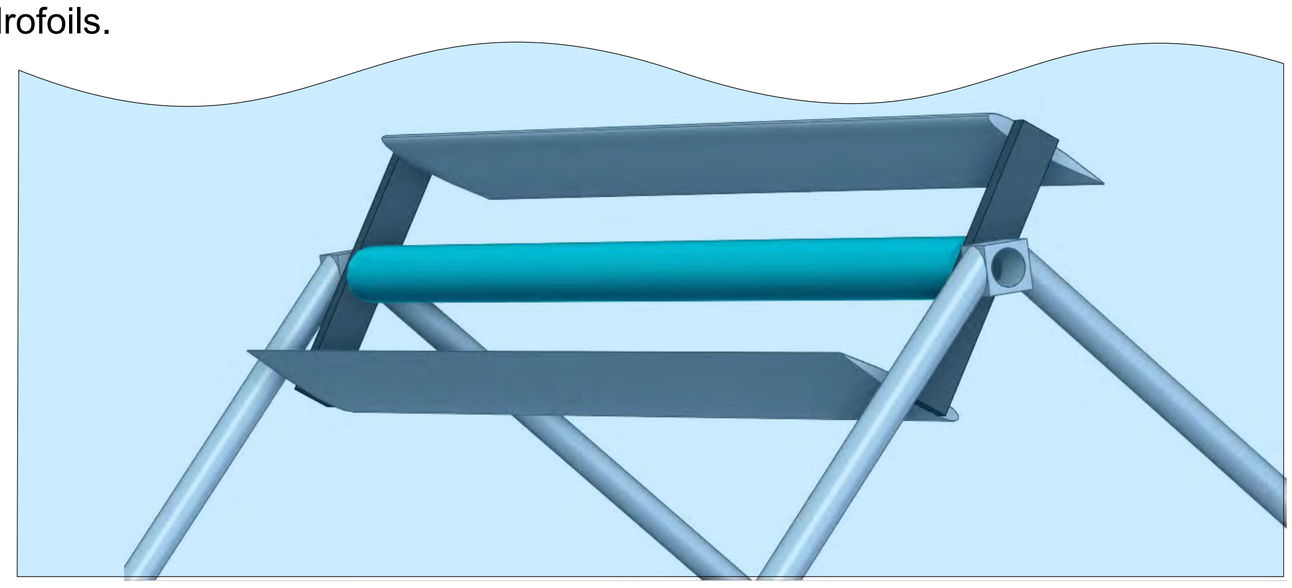

Figure 2. LiftWEC device under wave crest. The figure shows the hydrofoils, the central shaft, the radial spokes and the supporting frame.

Hydrodynamic model

Figure 3a shows a schematic of a phased-locked LiftWEC rotor with two hydrofoils. The rotor's velocity (u) is at 90 degrees with respect to that of the wave velocity (v). This generates a relative velocity (w) at an angle of attack (α), and therefore a lift (L) and drag (D) force on the hydrofoils. Figure 3b shows wave climate data from a point in the Atlantic Coast of France and the wave design conditions (Hs = 4 m, Ts = 10 s). Figure 3c shows a time series of the lift and drag coefficients subject to a regular wave at a water depth of 50 m and a 6 m submergence. The radius of the rotor is 10 m.

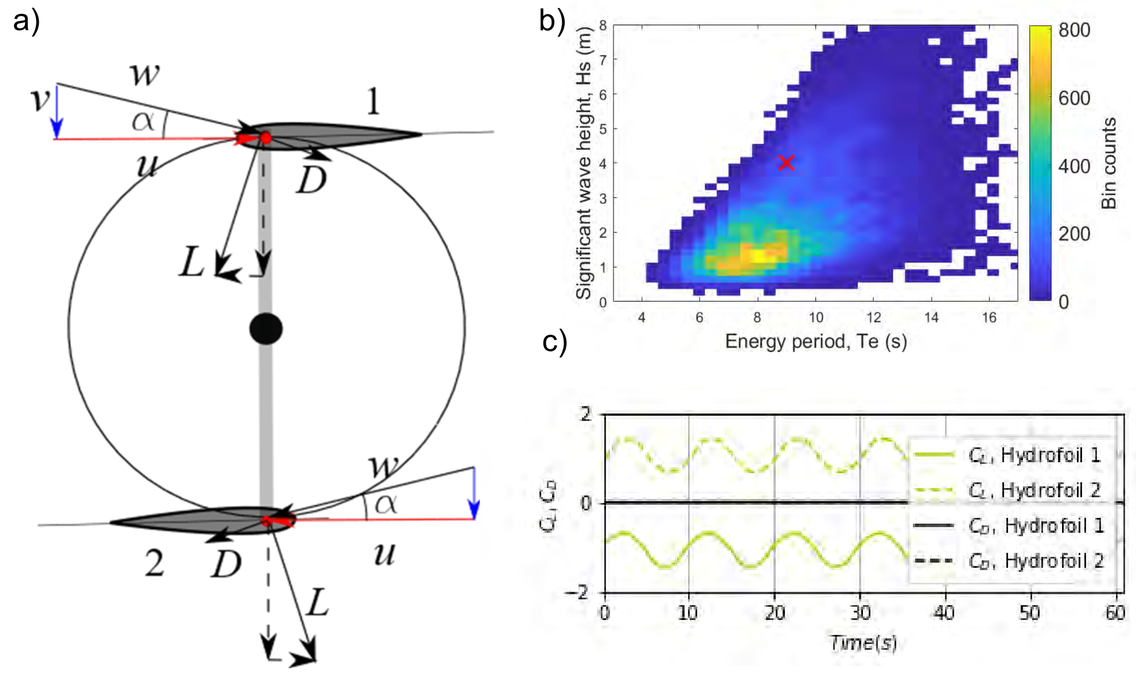

Figure3. a) Velocity vectors and forces of LiftWEC, b) wave data and design conditions from a point in the Atlantic coast of France and c) time sequence of lift and drag coefficients in two hydrofoil rotor

Structural design

A hollow-squared cross section was utilised to model the hydrofoil and two loading distributions were applied (uniform and linear). Figure 4a shows the case of uniform loading. The maximum load from the hydrodynamic model was distributed over the hydrofoil to compute the shear forces (V), bending moments (M), deflections (y) and bending stresses on the hydrofoils (figure 4b). Analytical solutions were derived for a doubly supported foil and a simply supported foil at the centre. The hydrodynamic and structural codes were coupled in Python to assess simultaneously the structural and hydrodynamic response to different wave conditions. It was found that LiftWEC is structurally resilient to design wave conditions, due to its submerged operation and passive stall when then stall angle is exceeded.

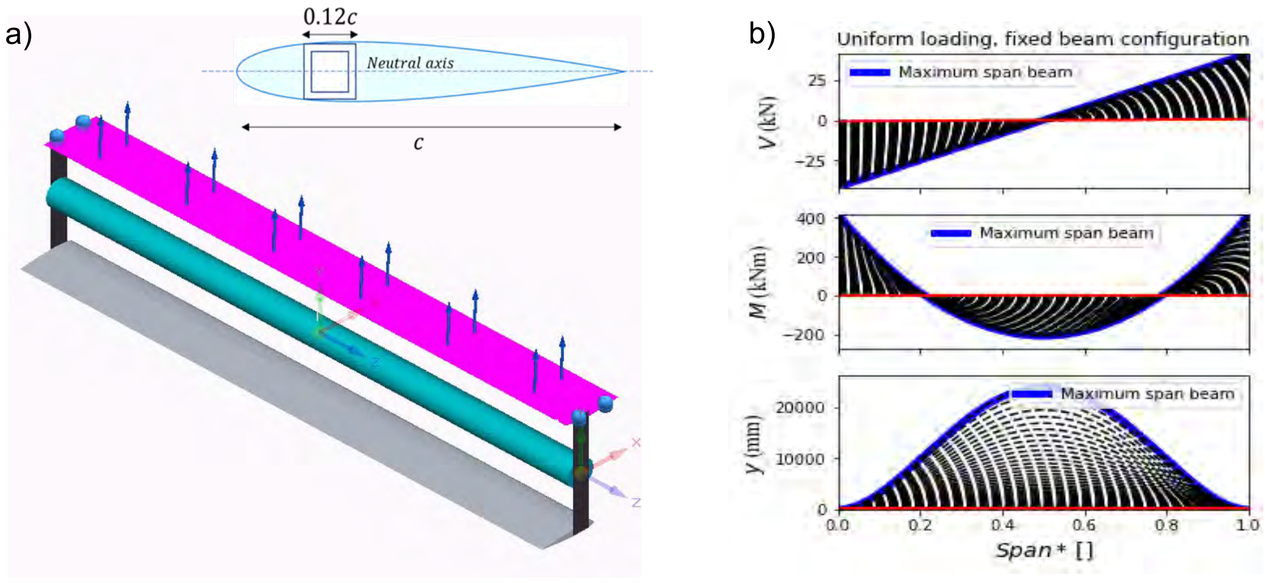

Figure 4. a) Uniform loading applied to a doubly supported LiftWEC and b) structural model and analytical results showing shear (V), bending moments (M) and deflections for variable span rotor (0 to 20 meters).

References

1. A methodology for the structural design of LiftWEC: a wave bladed cylcorotor (In preparation). Arredondo-Galeana, A.; Shi, W.; Olbert, G.; Scharf, M.; Ermakov, A.; Brennan, F. In the 14th European Wave and Tidal Energy Conference, 2021
2. Lift-based wave energy converters – an analysis of their potential. Folley, M.; and Whittaker, T. In the 13th European Wave and Tidal Energy Conference, 2019
3. P. Schmitt, T. Whittaker, D. Clabby, and K. Doherty, "The opportunities and limitations of using CFD in the development of wave energy converters," in RINA, Royal Institution of Naval Architects - International Conference on Marine and Offshore Renewable Energy, pp. 89–97, 2012.
4. Deep ocean wave energy conversion using a cycloidal turbine. Siegel, S., G.; Jeans, T.; and McLaughlin, T., E. Applied Ocean Research, 33(2): 110-119. 2011.

LiftWEC
www.liftwec.com
@LiftWEC

This project has received funding from the European Union's Horizon 2020 research and innovation programme under Grant Agreement No. 851885.

Investigation of offshore wind turbine performance within a wind farm

Xue Xu[1], Matthew Cole[2], Adam Stock[2], Maurizio Collu[1]

1. Department of Naval Architecture, Ocean and Marine Engineering, University of Strathclyde, Glasgow (xue.xu@strath.ac.uk)
2. Department of Electronic and Electrical Engineering, University of Strathclyde, Glasgow

University of Strathclyde Engineering

Introduction

- This study investigated each wind turbine performance within a 15 wind turbines wind farm.
- By investigating the aerodynamic wake effect within the wind farm, it can help to optimize the wind farm operation and maintenance, as part of the HOME-Offshore project (EP/P009743/1).

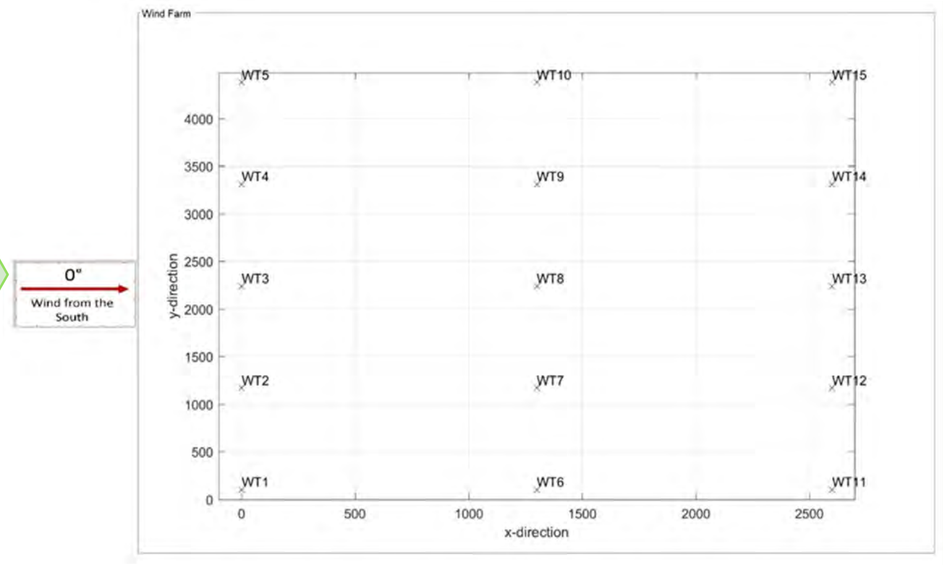

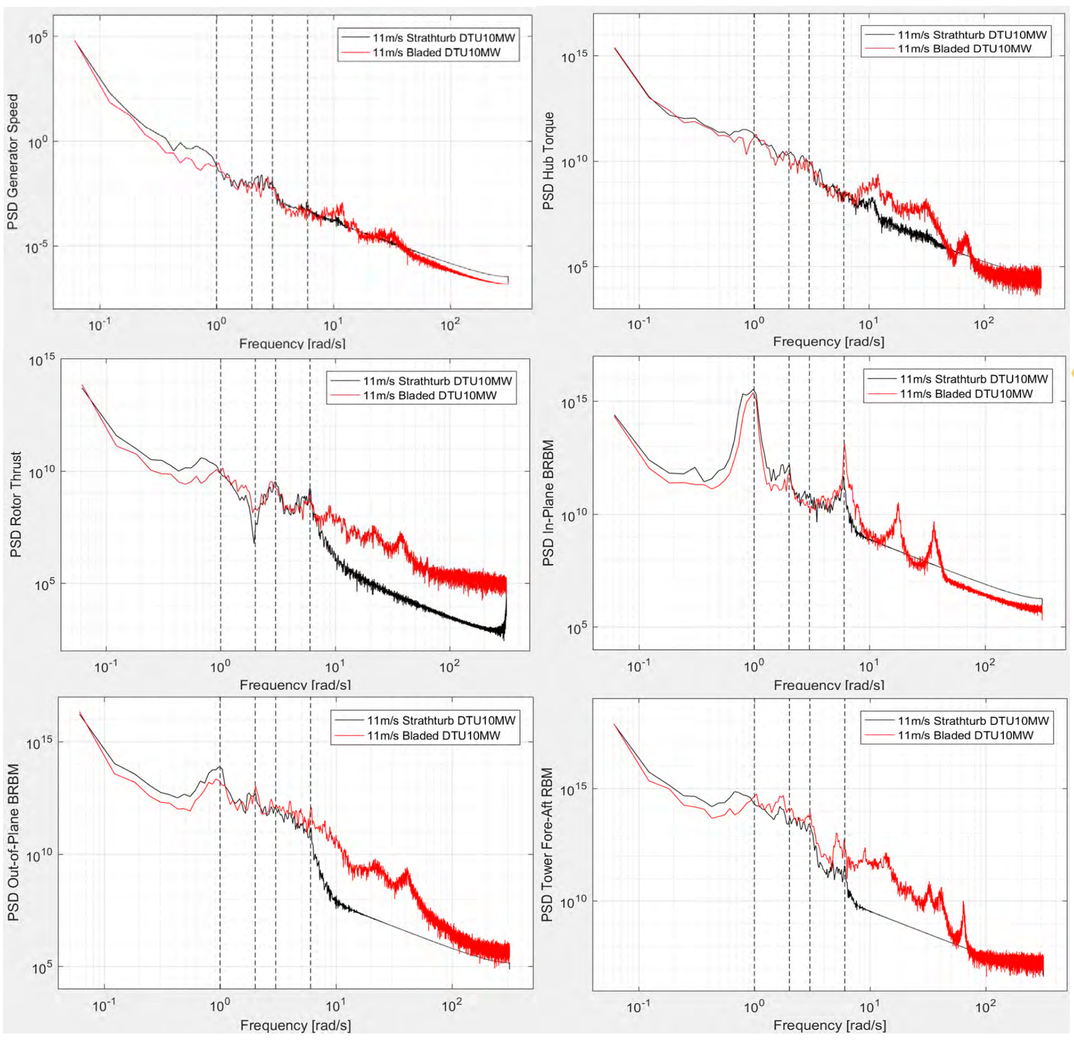

Methodology

- The wind farm modelling tool – Strathfarm is used in this study, which is developed in Matlab. Each load case with 900s physical time will take around 1hr 30mins~2hrs to run in Windows system with around 3.86Ghz and 5.8Gb RAM, which is much quicker than using CFD methods.
- Before input the turbine model into Strathfarm, the single turbine in Strathturb has been validated against Bladed, where good agreements are achieved.

Wind turbine performance predicted by Strathfarm

- WT model is the DTU10MW.
- Distance between WT1 to WT2 = 6*D; WT1 to WT6 = 7.3*D.
- Load cases been checked: 7.5m/s, 11.4m/s and 15m/s at four wind directions: 0deg, 30deg, 60 deg and 90 deg.
- Output results: generated power; actual wind speed/ turbulence intensity in front of each WT

Wind direction 0 deg →

Wind Speed = 7.5 m/s WIND SPEED @ WIND TURBINE		
WT5	WT10	WT15
7.39	6.94	7.01
WT4	WT9	WT14
7.35	6.97	6.93
WT3	WT8	WT13
7.43	7.02	6.83
WT2	WT7	WT12
7.41	7.02	6.87
WT1	WT6	WT11
7.44	7.02	6.91

Wind direction 0 deg →

Wind Speed = 7.5 m/s WIND TURBINE POWER GENERATED		
WT5	WT10	WT15
2.64	2.21	2.01
WT4	WT9	WT14
2.62	2.28	2.11
WT3	WT8	WT13
2.56	2.12	1.88
WT2	WT7	WT12
2.52	2.15	2.04
WT1	WT6	WT11
2.80	2.24	2.18

Wind direction 0 deg →

Wind Speed = 7.5 m/s TURBULENCE INT. @ WIND TURBINE		
WT5	WT10	WT15
0.15	0.16	0.16
WT4	WT9	WT14
0.14	0.17	0.16
WT3	WT8	WT13
0.14	0.15	0.17
WT2	WT7	WT12
0.15	0.16	0.17
WT1	WT6	WT11
0.14	0.15	0.16

Wind direction 90 deg ↓

Wind Speed = 11.4 m/s WIND SPEED @ WIND TURBINE		
WT5	WT10	WT15
11.31	11.40	11.35
WT4	WT9	WT14
10.68	10.70	10.60
WT3	WT8	WT13
10.47	10.45	10.49
WT2	WT7	WT12
10.43	10.37	10.35
WT1	WT6	WT11
10.40	10.30	10.41

Wind direction 90 deg ↓

Wind Speed = 11.4 m/s TURBULENCE INT. @ WIND TURBINE		
WT5	WT10	WT15
0.12	0.12	0.12
WT4	WT9	WT14
0.14	0.13	0.14
WT3	WT8	WT13
0.14	0.14	0.14
WT2	WT7	WT12
0.14	0.15	0.15
WT1	WT6	WT11
0.14	0.15	0.14

Wind direction 90 deg ↓

Wind Speed = 11.4 m/s WIND TURBINE POWER GENERATED		
WT5	WT10	WT15
8.50	8.42	8.45
WT4	WT9	WT14
7.39	7.51	7.37
WT3	WT8	WT13
7.29	7.16	7.08
WT2	WT7	WT12
7.15	7.15	7.21
WT1	WT6	WT11
7.15	6.82	7.08

Wind direction 30 deg ↘

Wind Speed = 15 m/s WIND SPEED @ WIND TURBINE		
WT5	WT10	WT15
14.97	14.98	14.95
WT4	WT9	WT14
15.01	14.71	14.67
WT3	WT8	WT13
14.99	14.69	14.62
WT2	WT7	WT12
14.92	14.73	14.66
WT1	WT6	WT11
14.93	14.72	14.63

Wind direction 30 deg ↘

Wind Speed = 15 m/s TURBULENCE INT. @ WIND TURBINE		
WT5	WT10	WT15
0.11	0.11	0.11
WT4	WT9	WT14
0.11	0.11	0.11
WT3	WT8	WT13
0.11	0.11	0.11
WT2	WT7	WT12
0.11	0.11	0.11
WT1	WT6	WT11
0.11	0.11	0.12

Wind direction 30 deg ↘

Wind Speed = 15 m/s WIND TURBINE POWER GENERATED		
WT5	WT10	WT15
9.94	9.97	9.96
WT4	WT9	WT14
9.89	9.82	9.83
WT3	WT8	WT13
9.86	9.80	9.72
WT2	WT7	WT12
9.87	9.85	9.79
WT1	WT6	WT11
9.92	9.82	9.76

Conclusion

- In this study, a medium fidelity model – Strathfarm, have been employed to investigate a 15 wind turbine wind farm performance under various wind speeds/directions. The DTU10MW model has been used and validated by using Strathturb against Bladed, where good agreement have shown.
- The results of only three of the load cases – 7.5m/s at 0 deg, 11.4m/s at 90 deg and 15m/s at 30 deg, are presented. It is discovered that when the wind direction is perpendicular to the wind farm, i.e. 0 deg or 90 deg, the reduction of the power generated at the back of the wind farm is more significant compared with the wind direction is at 30 deg.

HOME Offshore

UKRI Engineering and Physical Sciences Research Council

Additive Manufacturing of Hybrid Metal-Composite Joints for Renewable Energy Applications

Dr. Saeid Lotfian
Dr. Francisca Martínez Hergueta
Prof. Athanasios Kolios

Engineering and Physical Sciences Research Council

CAMREG Centre for Advanced Materials for Renewable Energy Generation

University of Strathclyde Engineering

Background

Conventional processes to join dissimilar materials, particularly metal and composite parts, result in very poor mechanical performance and durability, and in addition, hinder the integration of composites in different renewable energy applications. The design of hybrid joints to ensure dissimilar materials present a similar load carrying capacity is a demanding optimisation exercise. Furthermore, renewable energy structures usually operate under extreme environmental conditions (pressure, seawater, temperature, humidity); thus, the understanding of the mechanical behaviour and durability of the joints is essential. The emerging additive manufacturing (AM) technologies present an attractive prospect to produce bespoke joints for hybrid structures.

Research Aim and Objectives

The main research goal of the project is to develop a novel approach to join dissimilar materials by means of additive manufacturing for metal components and 3D printed composites – and to provide a quantified basis towards establishing new guidance to design hybrid composite/metal joints with improved structural efficiency for extreme environmental conditions. The three partial objectives are:

- Development of a 3D printed composite/metal hybrid joint.
- Thermo-mechanical characterisation of the hybrid joints.
- Risk evaluation and technology qualification plan.

Also, a numerical tool will be developed and validated against experimental results to predict the mechanical response of critical components.

Simulation results

The computational and simulation study has been done for different hole pattern assembly:

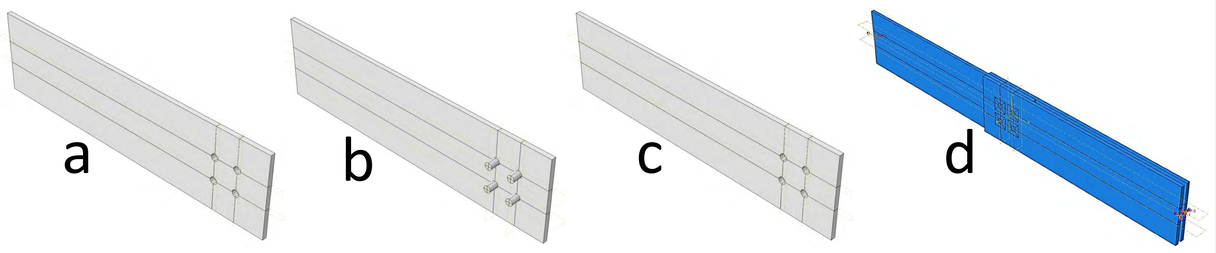

2×2 Hole Pattern Assembly Simulation, (a) Composite; (b) Metal sheet with pins; (c) Metal sheet; (d) Interaction and Load.

Force vs. Displacement graph

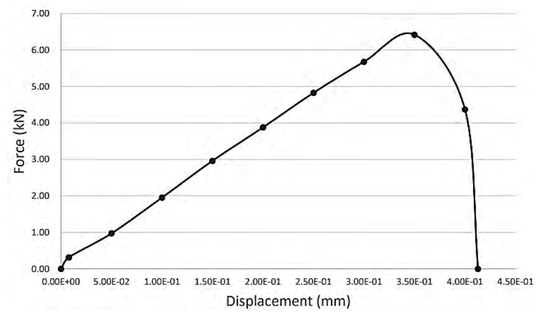

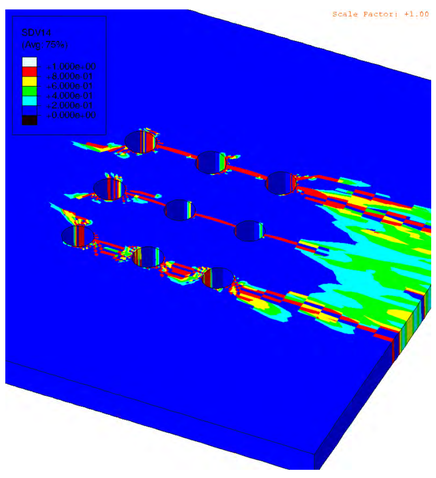

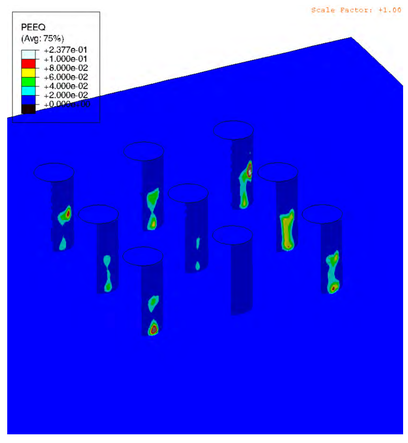

(*left*) *the figure shows that the matrix of the composite has been cracked;* (*right*) *the figure shows that the pins on the metal sheet has been plasticized.*

Collaborators

AFRC Advanced Forming Research Centre, University of Strathclyde; institute IMDEA materials; NIT New Infrared Technologies; babcock; CATAPULT High Value Manufacturing

Acknowledgements

We would like to acknowledge the financial support from the Engineering and Physical Sciences Research Council (EPSRC) through Centre for Advanced Materials for Renewable Energy Generation (CAMREG) project.

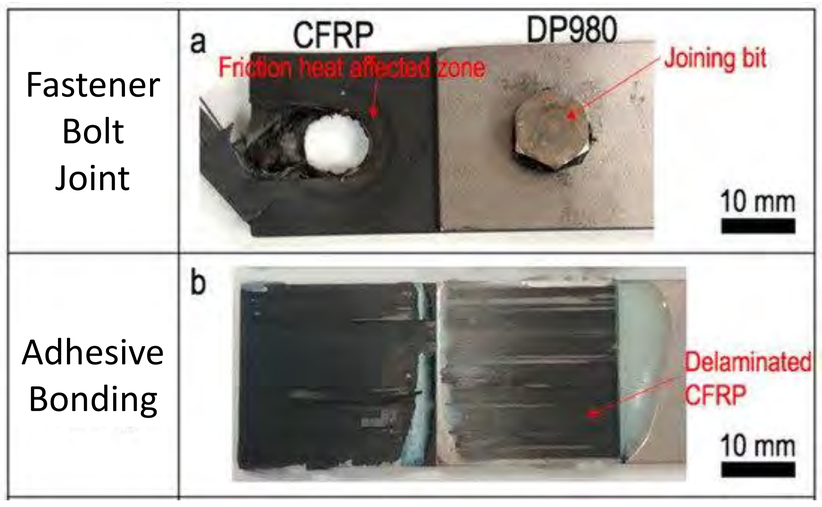

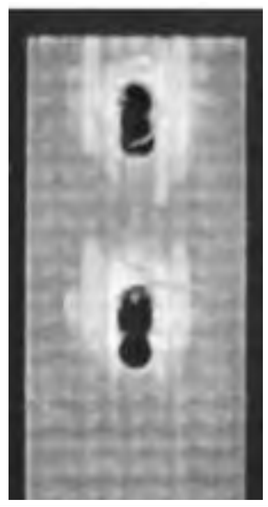

Manufacturing and Assembling

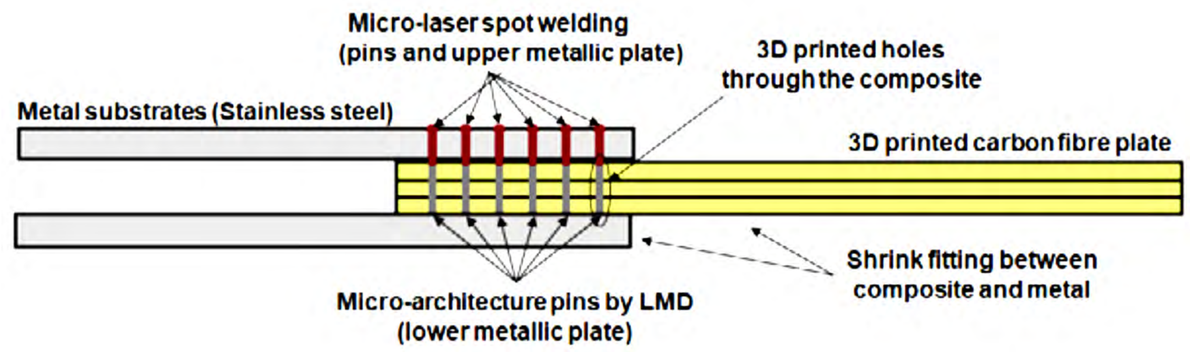

Manufacturing & assembling details

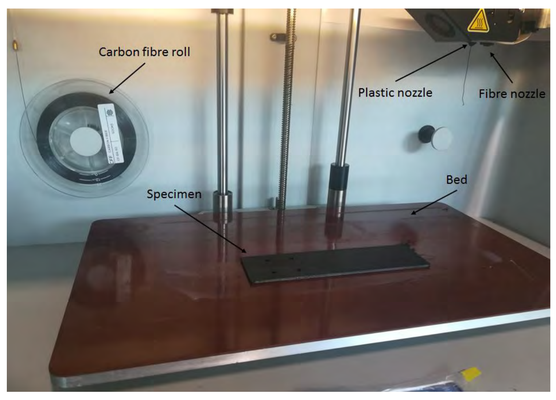

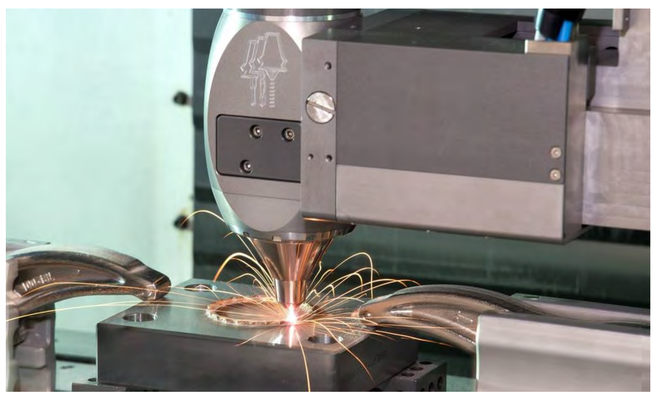

(*left*) *MarkForged II Desktop composite 3D printer;* (*right*) *Hybrid Manufacturing Technologies, Laser Metal Deposition (LMD) equipment*

(*a*) Fibre reinforcement strategy; (b) Circular fibre reinforcement; (c) SEM micrograph at x80 magnification.

AM allows the manufacturing of reinforced holes with concentric fibres, supressing the drilling operations during assembly of composite components.

Challenges

- Reducing number of defects in 3D printed composites
- Assessing damage on substrates due to the spot welding process
- Prediction of the mechanical response
- Identify and prioritise the risks of the newly proposed solution
- Comparing its performance with conventional solutions
- Informing the inspection strategy through analysing failure mechanisms of prevailing failure modes, specifying the inspection methods and intervals through a reliability-centred maintenance approach.

Relevant References

1.Guo, N. and M.C. Leu, *Additive manufacturing: technology, applications and research needs.* Frontiers of Mechanical Engineering, 2013. **8**(3): p. 215-243.
2. *Additive manufacturing UK national strategy 2018-25.* 2017, AM-UK Steering Group.
3. Furumoto, T., et al., *Monitoring of laser consolidation process of metal powder with high speed video camera.* Physics Procedia, 2012. **39**: p. 760-766.
4. Gu, D., et al., *Laser additive manufacturing of metallic components: materials, processes and mechanisms.* International materials reviews, 2012. **57**(3): p. 133-164.
5. Lotfian, S., et al., *Chemically graded Fe–Al/steel samples fabricated by laser metal deposition.* MRS Advances, 2017. **2**(26): p. 1393-1398.
6. Bandyopadhyay, A. and B. Heer, *Additive manufacturing of multi-material structures.* Materials Science and Engineering: R: Reports, 2018. **129**: p. 1-16.

The potential and challenges of using drones to measure surface currents at tidal stream sites

Iain Fairley *i.a.fairley@swansea.ac.uk, Energy and Environment Research Group, Faculty of Science and Engineering, Swansea University, SA1 8EN, U.K.*

Introduction

- Current measurement at tidal stream sites are costly, high risk and require specialised equipment (ADCPs, vessels)
- An alternative low-cost, low-risk approach could be to derive surface currents from drone collected video (Figures 1 & 2) and processed with large scale particle image velocimetry
  - Achieved in the fluvial domain, e.g [1]
- UK regulations allow drones to be flown up to 500m from operator and at a height of up to 122m; raising possibility of land-based operations at potential tidal energy sites.
- Survey vessel not required; suitable for rapid deployment at remote sites
- Provides a spatial map rather than point measurement,
  - Image footprint 119 x 67m (24mm lens at 120m)
- Several challenges that need to be overcome compared to fluvial domain:
  - Georectification without ground control points
  - Lack of physical tracers (leaves, foam patches etc.)
  - Non-uniform tracer distribution
  - Wave signature obscuring current signature

Figure 1: Drone being flown at META test site, Pembrokeshire (photo credit: Marine Energy Wales)

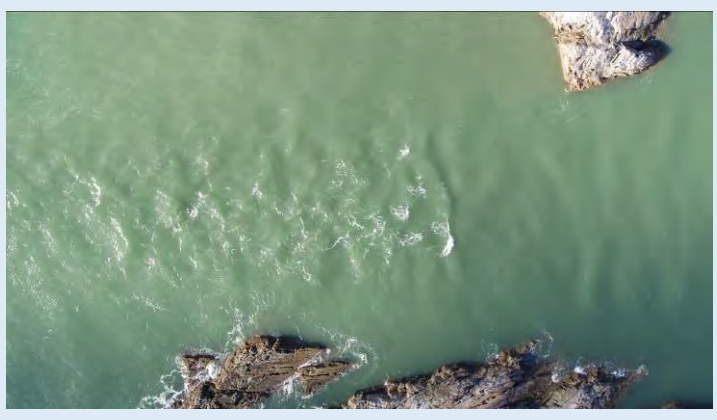

Figure 2: Example video frame from drone at 120m above surface at Swansea Bay trial site

Image georectification

- Fixed ground control points for image georectification not necessarily in field of view for tidal stream sites
- Therefore proposed georectification method is:
  - Set gimbal pitch to -90 (directly downward) and assume constant pitch
  - Use compass heading and GPS log to calculate drone movement; convert to pixel shift of undistorted image based on ground pixel size
- Initial tests comparing (non RTK-) GPS calculated pixel shifts to shifts calculated with cross-correlation of templates using fixed features (actual image shift) shows GPS accuracy may not be sufficient to describe drone movement while hovering (Figure 3).
  - However frame to frame movement is small and hence may not dramatically increase error in calculated velocity.
- Further test planned for a range of wind speeds and including using higher accuracy RTK-GPS for drone position

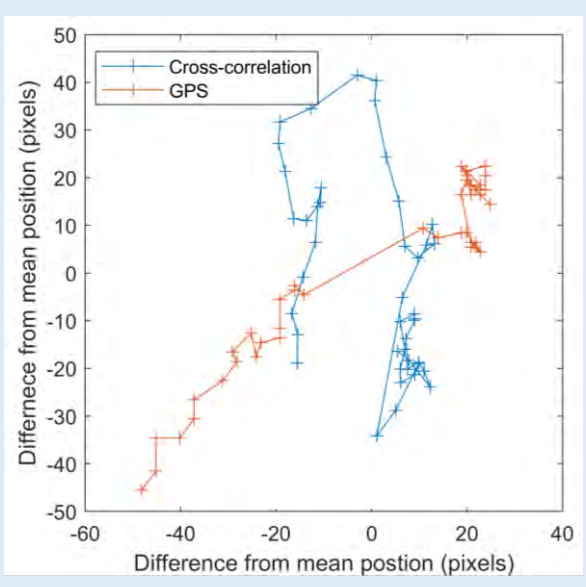

Figure 3: An example comparison between non-RTK GPS derived image shift in pixels and the real image shift in pixels based on cross-correlation. Each point is separated by 2s. Windspeed was 10mph.

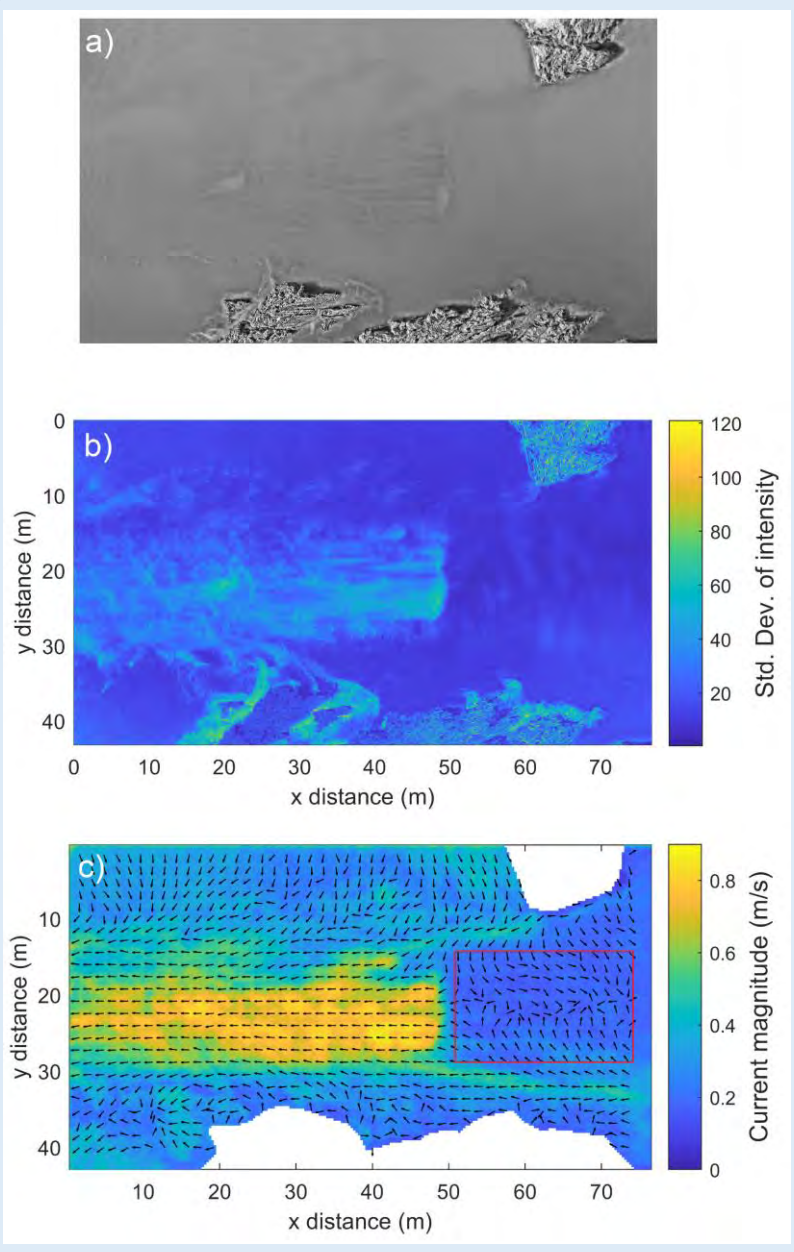

Figure 4: a) A mean image from 10s of video data, lighter areas indicate greater proportion of foam patches; b) standard deviation in grayscale intensity; c) current magnitude and direction calculated using PIVlab [2] with 10s of video at 29.97fps.

Image complexity and pre-conditioning

- Unlike fluvial studies, tracers largely comprise of surface texture and foam patches; distribution of foam patches depends on wave breaking (Fig. 4).
- Low tracer areas show much higher spurious correlations which leads to suspect velocities (Fig. 4c) when basic images used in PIVlab [2]
  - Low velocities and reversed direction highlighted by red box in 4c, which is does not match visual interpretation of data
  - Raises question of whether different pre-processing should be applied to different sections of images for complex sites.
- In wave exposed areas, wave signatures can be of similar magnitude to current patterns (Figure 5).
- Empirical mode decomposition and contrast stretching seems to hold some promise to both remove waves and emphasize currents patterns in low tracer regions (Figure 5).

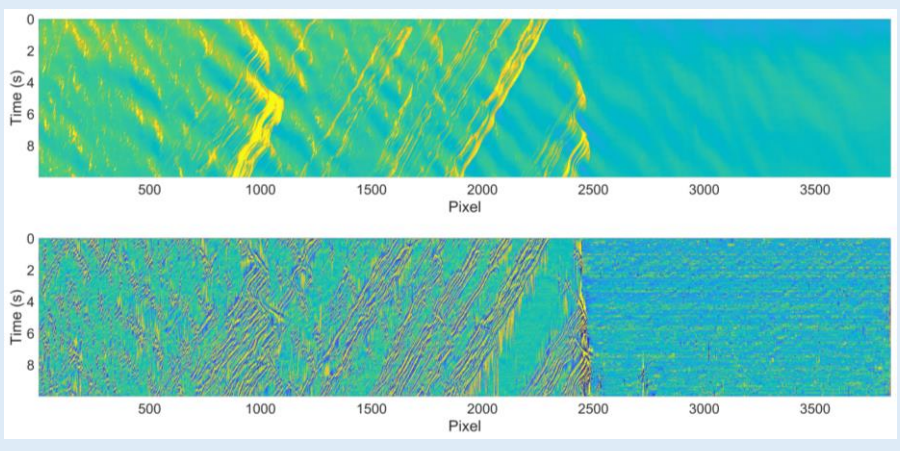

Figure 5: Pixel timestacks of false colour greyscale intensity from a transect through the centre of the image (y=22m in Fig. 4) for the raw (upper) and optimized (lower) images. Current direction is from right to left and wave direction from left to right. Removal of wave signature and clearer current patterns for pixels above 2500 can be seen in the lower panel.

Ongoing and Future Work

- EU ERDF funded Selkie project is assessing existing PIV tools and developing image collection and processing workflows to enable robust drone-based current measurements at tidal stream sites
  - Establish accuracy of drone hovering and GPS based georectification in land-based experiments to quantify uncertainty in surface currents caused by variation in 3D drone position
  - Explore techniques to pre-condition video; enhancing current signatures and removing waves and other unwanted surface features (to be presented at EWTEC2021)
  - Test a range of open source particle image velocimetry and particle tracking velocimetry tools
- EPSRC Supergen ORE Flex Fund project V-Scores will provide a comprehensive validation of techniques and assess the relationship between surface currents and currents at turbine-relevant depths
  - Fieldwork at two sites: Ramsey Sound, Pembrokeshire, and Inner Sound, Pentland Firth

References and Acknowledgements

The Selkie Project is funded by the European Regional Development Fund through the Ireland Wales Cooperation programme.

[1] Tauro et al. 2016. Assessment of drone-based surface flow observations. Hydrological Processes 30, 7

[2] Thielicke, W. and Stamhuis, E.J. (2014): PIVlab – Towards User-friendly, Affordable and Accurate Digital Particle Image Velocimetry in MATLAB. Journal of Open Research Software 2(1):e30, DOI: http://dx.doi.org/10.5334/jors.bl

Supergen Offshore Renewable Energy

UKRI Engineering and Physical Sciences Research Council

ERDF Llywodraeth Cymru Welsh Government Ewrop & Chymru: Buddsoddi yn eich dyfodol Europe & Wales: Investing in your future European Regional Development Fund

SELKIE

EU Funds: Ireland Wales Programme 2014-2020

Swansea University Prifysgol Abertawe

Plate anchors for offshore floating facilities – Soil – anchor – floating system interactions

UNIVERSITY OF Southampton

Dr Katherine Kwa & Prof David White

Background

The embedded plate anchor and mooring system is an efficient and versatile deep water foundation solution for floating offshore renewable energy structures (Fig.1a & b). It can be used as the example anchor type to illustrate more general features of seabed behaviour. The capacity of this anchoring system is enhanced by the strength and weight of the surrounding soil which resists uplift of the plate.

It is essential to have a reliable estimation of the uplift capacity that the plate anchor can provide for the variety of loads that are transmitted via the mooring lines to the anchoring system.

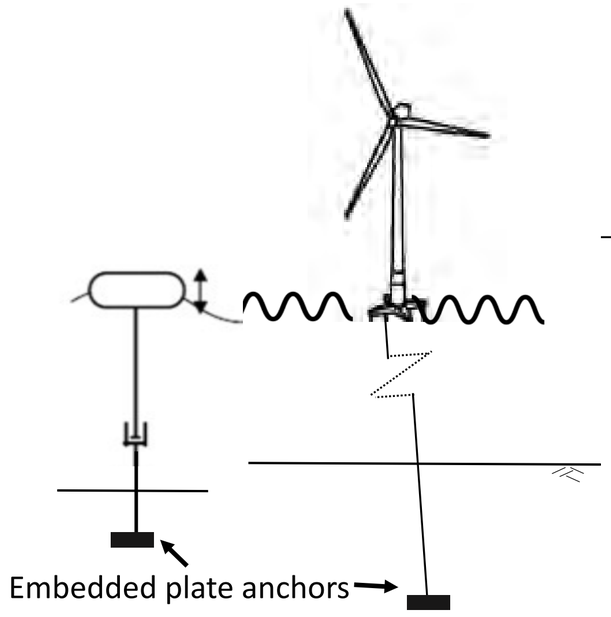

Figure 1a: The embedded anchor and mooring system

Figure 1b: Types of embedded anchors

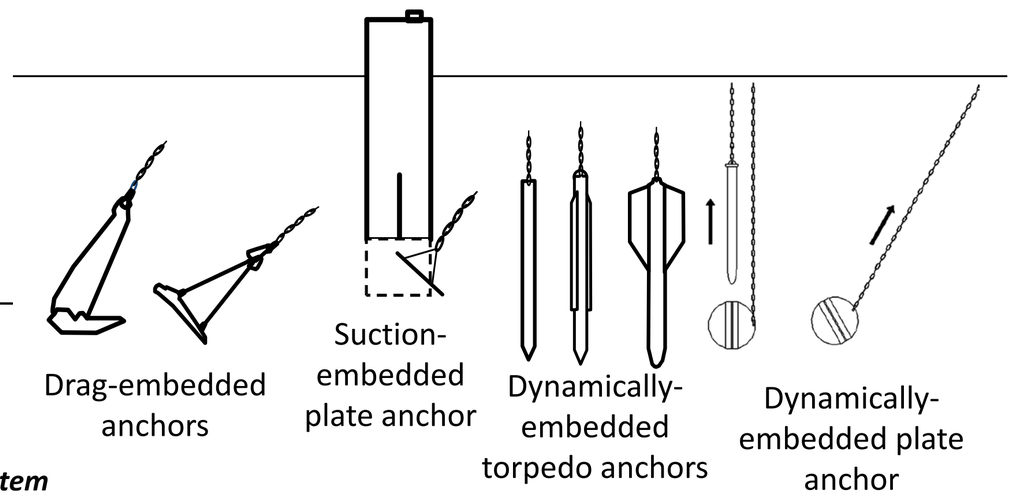

Aim

This project integrates seabed-anchor interactions into mooring analyses to gain a better understanding of the full response of floating offshore renewable energy (FORE) facilities (Fig. 2a).

Methodology

The project uses the emerging concept of **whole-life geotechnical design** to couple the life cycle of imposed actions with the evolving geotechnical seabed resistance due to consolidation effects, with seabed-anchor structure responses across the design life of the FORE infrastructure. In soft soils, the capacity of an anchor can change with time due to the sustained loads and variable components of the cyclic uplift loads. These loads depend on the sea state, season and the connected FORE facility. These long-term changes in the *static* geotechnical soil effects can be simply described and integrated into existing mooring analyses via spring-slider relationships (Fig. 2b).

During the application of higher frequency loads (eg. snatch loads), there are viscous and inertial or **added mass** effects from the mass of the seabed soil surrounding the anchoring systems, which can result in significant increases in the *dynamic* anchor capacity. These added mass effects in soil are overlooked in anchor design, but are well understood and applied in hydrodynamics. In this project we have derived new added mass coefficients, N_{AM}, for soil failure, calculated from assumed shear based plastic failure mechanisms that mobilise around embedded plates anchors. Our new analysis shows that in soil, the added mass effect is approximately double compared to in inviscid fluid (Fig. 2c).

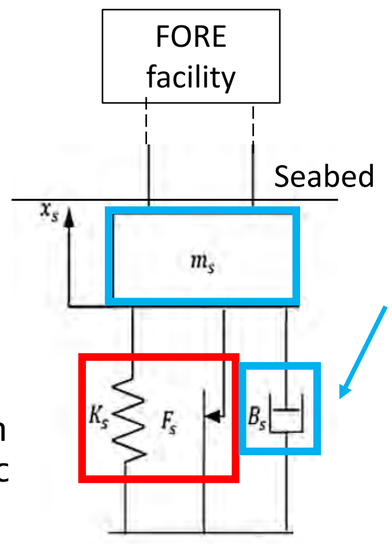

Figure 2a: Schematic of the Integrated seabed-anchor mooring model

Spring-Slider:

Long term, **'whole-life'** changing geotechnical seabed strength (s_u)

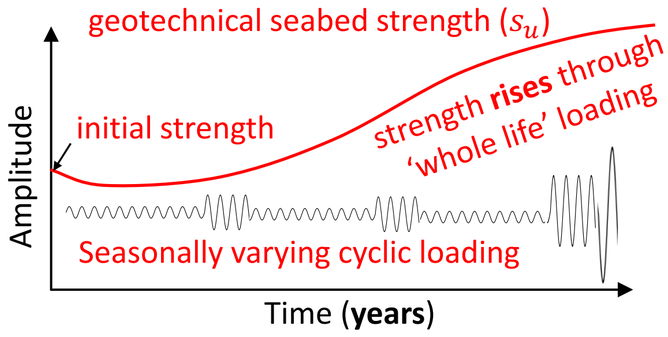

Figure 2b: Whole-life geotechnical response

Added Mass & Viscous Effects:

B: anchor diameter
a: acceleration
ρ: density

N_{AM}: dimensionless hydrodynamic added mass coefficient

$$F_{AM} = N_{AM}\rho B^2 a$$

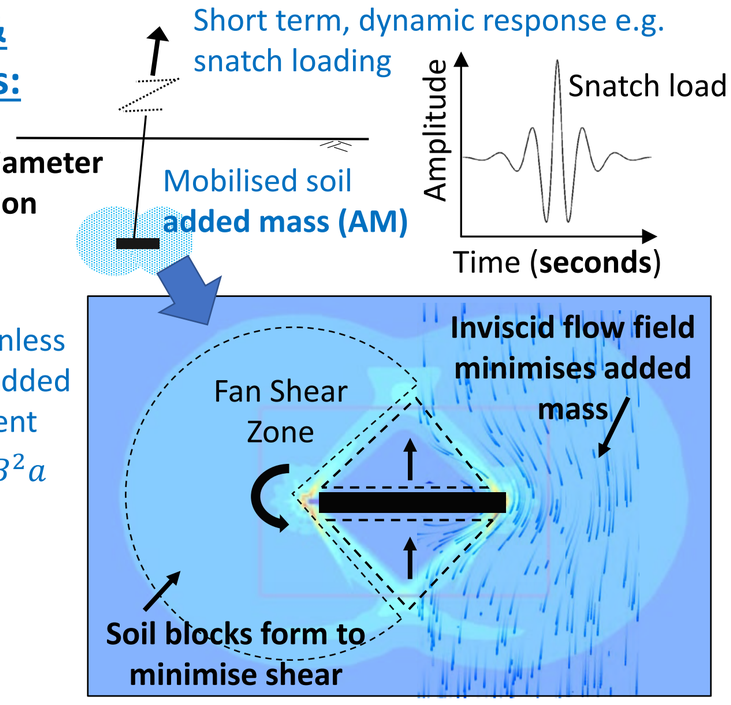

Key observation: **Different** mobilised plastic failure mechanisms in **soil** vs **fluid** (inviscid flow). The resulting effect of **added mass in soil is significant** compared to in fluid.

N_{AM}	2D Plane Strain Plate	3D Circular Plate
Hydrodynamics	0.79	0.33
Geotechnical	1.648	0.548

Double

Figure 2c: Comparison of mobilised failure mechanisms

Application

Preliminary simulations from a developing soil-anchor interaction model show significant anchor capacity enhancements as a result of whole-life consolidation effects, and from dynamic added mass and viscous effects (Figs. 3a & b). Allowing for these positive whole-life changes in seabed strength and the added mass and viscous effects unlocks beneficial design outcomes. It offers opportunities for more cost effective and efficient anchoring systems resulting in reductions in anchoring size, reduced risk of fatigue, greater insight for late life management and informed decommissioning processes for FORE infrastructure.

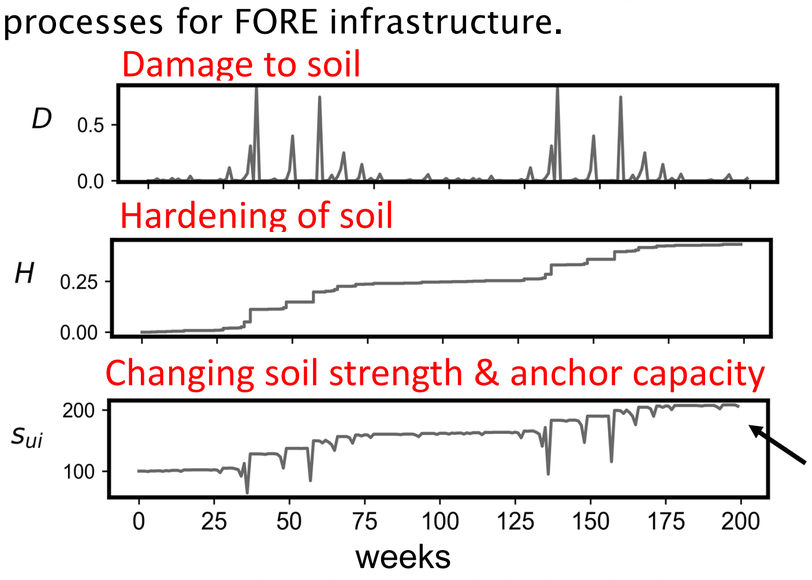

~2x gain in soil strength & anchor capacity **over 4 years**

Figure 3a: Changing geotechnical seabed response

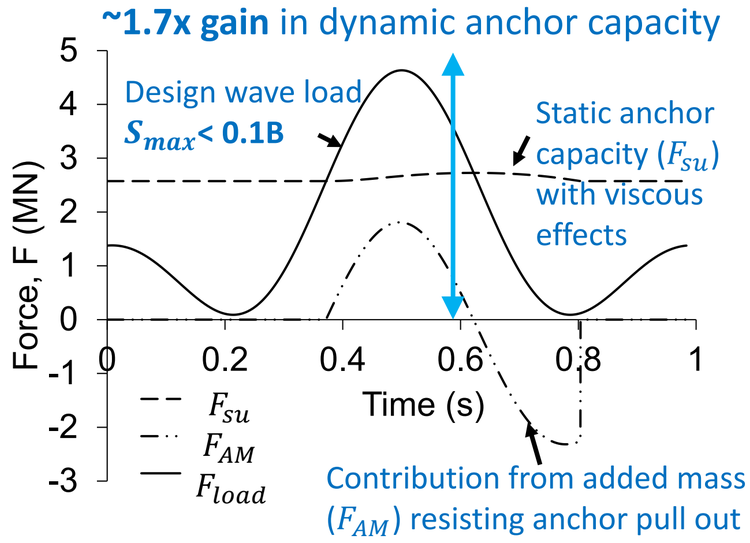

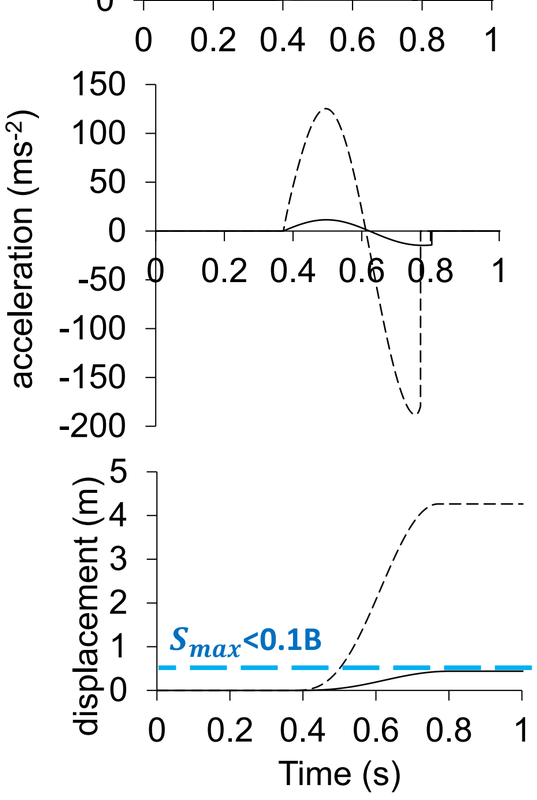

Figure 3b: Added mass and viscous effects on dynamic anchor capacity and response

Future Work

We are in the process of calibrating and validating the developing soil-anchor model, and packaging it into a form that will couple with existing floating system models. Future work aims to create a fully integrated seabed-anchor-mooring engineering design tool that can be used in practice to improve anchoring design for FORE facilities.

Further Reading: Kwa et al. (In press) *Analysis of the added mass term in soil bearing capacity problems* Geotech. Lett; Laham, Kwa, et al. 2020. *Episodic direct simple shear tests to measure changing strength for whole-life geotechnical design* Géotech. Lett.; Kwa & White (submitted*) Plate anchors for floating offshore facilities: soil-anchor-floating system interactions* 20th ICMGE. Syd, Aus ; Kwa et al. (In Progress) *Enhanced capacity of embedded plate anchors due to consolidation under sustained load.*

Supergen Offshore Renewable Energy

EPSRC Engineering and Physical Sciences Research Council

Email: k.a.kwa@soton.ac.uk

Supergen ORE Hub Annual Assembly
18th-22nd January 2021

Supergen Annual Assembly 2021

Impact of spatially varying onset flow conditions on loading of a tidal turbine

H. Mullings T. Stallard

hannah.mullings@manchester.ac.uk, Department of Mechanical, Aerospace and Civil Engineering,

The University of Manchester, United Kingdom

Aim

To establish the range of fatigue load predictions which can exist for equivalent quasi-steady onset flow conditions.

Background

Objectives

- *Demonstrate load prediction through the use of synthetic turbulence spectra.*
- *Examine the influence of operating conditions on the design life of tidal turbines.*
- *Establish variation in loads at different positions within a site using an efficient blade element method.*

Motivation

Tidal turbines experience a range of unsteady onset flow conditions due to their locations and the surrounding environment. Design standards currently consider onset flow conditions measured from a single device (ADCP) located 1-2D from a potential turbine position. This study quantifies the extent to which a small spatial variation will impact the onset flow which is simulated, examining a small range of conditions which are considered to have the same disk averaged velocity (U_{DA}) but result in different unsteady loads. The conditions at these measurement points are considered as input to an efficient blade element model to determine the variation of loading with location and position.

Modelling Methods

Onset Flow Modelling

Considering the design standards [1] 'normal' conditions should be considered as the basis for calculating fatigue loads.

Normal conditions are determined by 10 minute mean stream-wise velocity, measured over the rotor plane which should include:

- *Shear Profiles*
- *Turbulence*
- *Waves*
- *Wakes*

Reference velocity calculated as a power weighted average using vertical ADCP measurements. This study initially considers the influence of turbulence and shear profiles on a range of measured onset flow points. The measurements were gathered as part of the ReDAPT project [2].

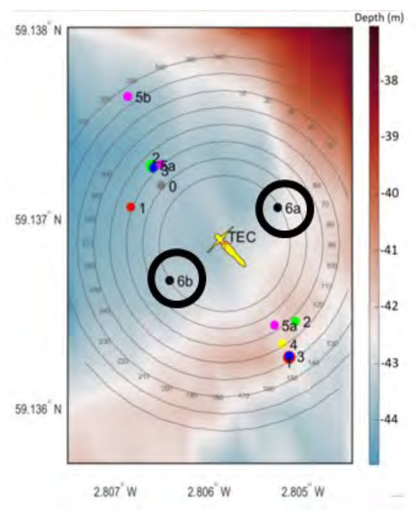

Figure 1: Locations of ADCP deployments during the ReDAPT project, two locations of interest are circled. Obtained from [2].

Load Modelling

- *Loads are modelled using stochastic frozen turbulent fields. Initially two different generation methods have been analysed a von Karman spectra and the Synthetic Eddy Method (SEM). These turbulent fields allow the determination of the relative onset flow experienced by the turbine blade.*
- *Fatigue loads are quantified using Damage Equivalent Loads (DEL) , defined in [3].*

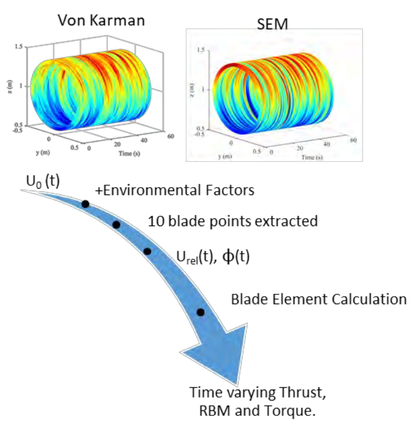

- *Load spectra compared to experimental measurements from XMED project [4].*
- *Additional 'blade scale flow' influence on loads included—determined from 2D CFD computations of C_L and C_D variations with unsteady onset flow to a blade segment. Interested in the separation frequency and gradient of lift and drag due to different onset flow conditions.*

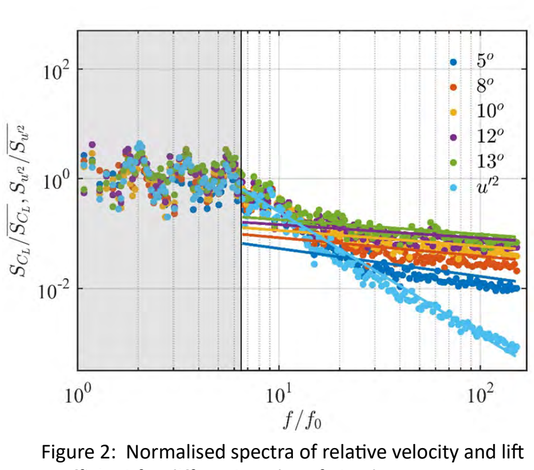

Figure 2: Normalised spectra of relative velocity and lift coefficient for different angles of attack.

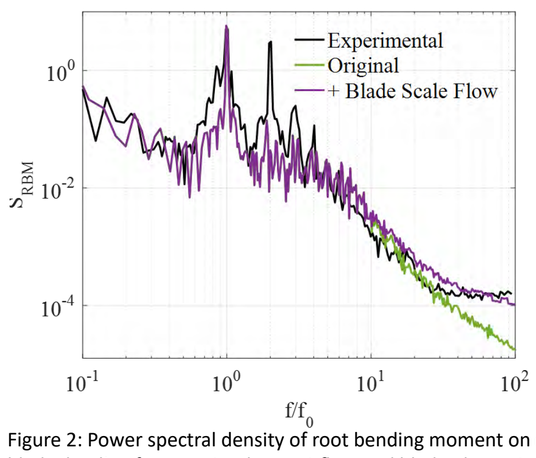

Figure 2: Power spectral density of root bending moment on one blade, loading from unsteady onset flow and blade element model and with the same model and the addition of the magnitude of high frequency fluctuations given.

Resource

- *Two synchronous measurement points approximately 2D from a turbine position, shown in Figure 1.*
- *Two vertical turbine positions are examined: (top floating hub =28m, bed-mounted hub = 15m).*
- *One range of reference velocity is used—1.8-2.0 m/s.*
- *Turbulence characteristics show a difference in average integral lengthscale for each location and position, turbulence intensity defined as fluctuation intensity which includes the influence from any waves.*

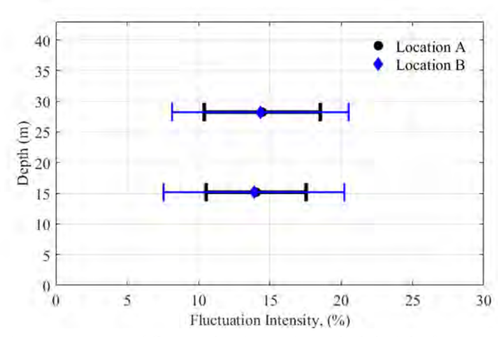

Figure 5: Range of fluctuation intensity at hub height for each turbine location and position.

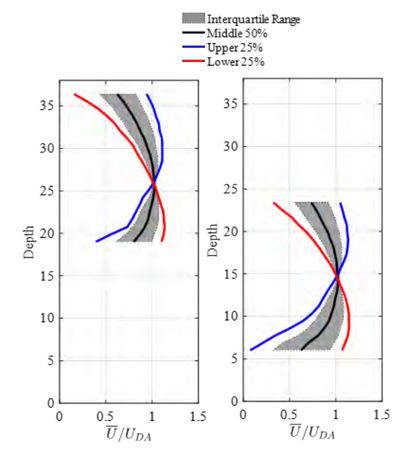

Figure 4: Range of shear profiles present at one site location for the two turbine positions.

Lengthscales	Location A	Location B
Top Position (28m)	9.78 m	7.36 m
Bottom Position (15m)	6.82 m	3.65 m

Results

- *Good agreement of overall spectral shape.*
- *Prediction of **peak load** at f_0 **within 4%.***
- *Prediction of damage equivalent load **within 22%**, with no blade scale flow fluctuations.*
- *Prediction of damage equivalent load **within 6%**, with blade scale flow fluctuations included.*
- *No shear applied ~13% higher loads at location B.*
- *Increase of 12% with average shear used for the top turbines*
- *Increase of 7-8% for the bottom turbine position.*

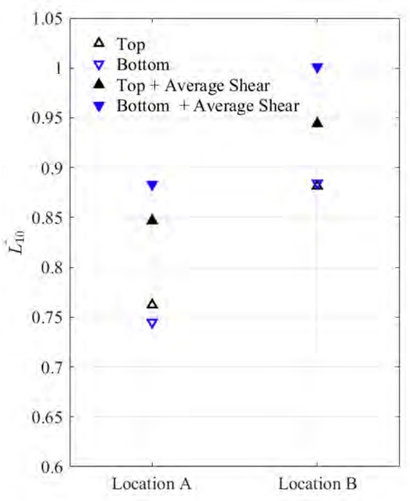

Figure 5: Variation of DEL for different onset flow conditions , turbine positions and locations.

Conclusions

- *Efficient method to determine blade loading shown.*
- *Preliminary results show variation in turbine position has a greater influence on loads than turbulence method.*
- *Characterisation of the onset flow based on spectra of U_{REL} at a blade radius of 0.7R.*

References

[1] DNV-GL Standard Tidal Turbines, DNV-GL-ST-0164, 2015.

[2] B. Sellar, V. Venugopal, D. Ingram and G. Wakelam in *Energies,* vol. 11, pp. 176, 2018.

[3] Parksinon and collier and ref.

[4] G.S. Payne, T. Stallard, R. Martinez and T. Bruce in *Journal of Fluids and Structures,* vol. 83, pp. 156-170, 2018.

Topside Bridge effect on the dynamic response of multi-purpose offshore platform under extreme condition

Dr. Yan Gao[1], Dr Maurizio Collu[1]

1- Naval Architecture, Ocean and Marine Engineering, University of Strathclyde, Glasgow

Introduction

An environmentally friendly multi-purpose offshore platform is developed by 'the Blue Growth Farm' (BGF) [1] project (Programme H2020-EU.3.2.5), which includes a square-shaped concrete platform, a wind turbine, a set of wave energy converters, and an aquaculture system. This multi-purpose offshore platform is well suited for open sea farm installation in terms of the Blue Growth Industry. This poster presents an investigation of the topside bridge effect on the response of the BGF platform under wind with high speed.

Numerical simulation

- An aero-hydro-elastic numerical model in SIMA[2].
- Model includes a wind turbine, a mooring system, a platform foundation, and a simplified topside bridge.

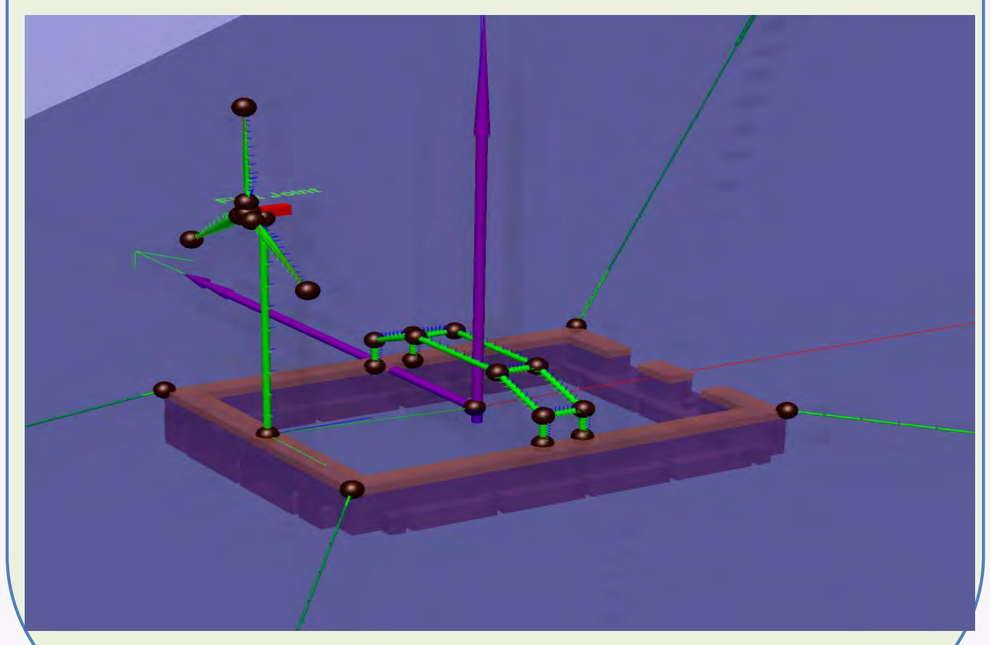

Numerical model with bridge

Conclusions and Future work

- Numerical analyses for the multi-purpose platform have been conducted and validated by good agreements with the water basin experiment.
- Outdoor experiment will be carried out in the near future, and the numerical model will be updated accordingly.

Problem Description

- Investigate the effect of the topside bridge on platform dynamic response.
- Loading condition: wind speed v=110 km/h, different directions.
- Platform equilibrium position, mooring line tension force, natural period are outputted.

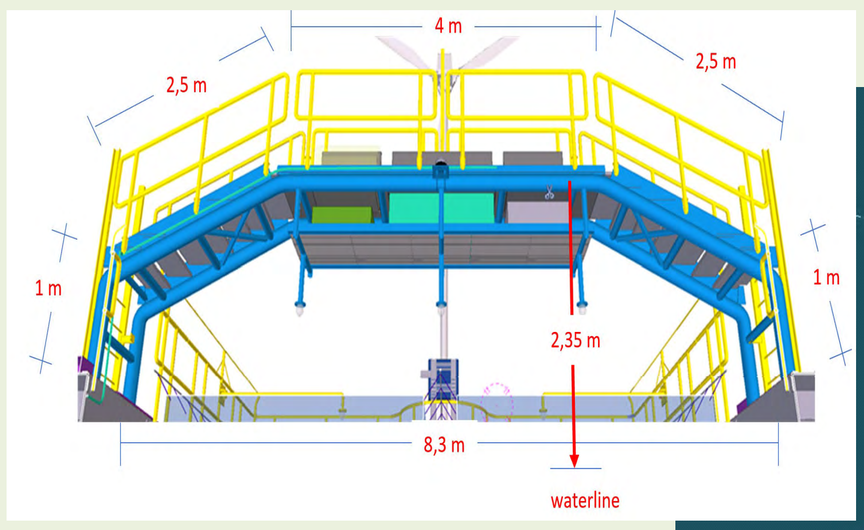

Bridge geometry

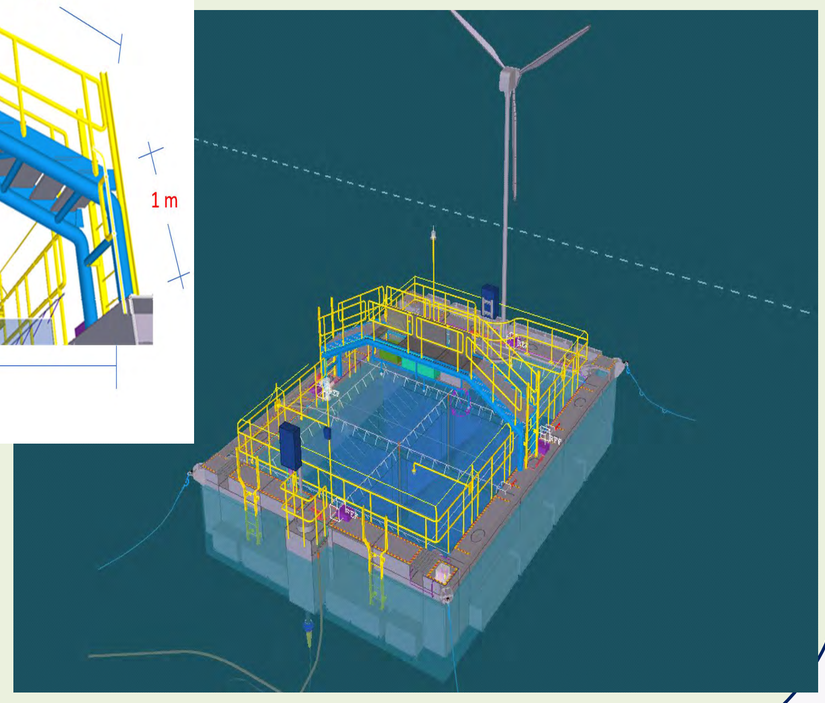

BGF platform with Bridge

With bridge ⟺ **Without bridge**

Results

Table 1 Bridge weight as 900 kg and wind direction **0** deg

	With bridge	Without bridge	Change
Natural period float	~29s	~29s	0
Equilibrium position (m)	(0.930,-0.0046,-0.033)	(0.457,-0.0044,-0.0018)	(0.473, -0.0002,-0.0312)
Mooring Line Force (N)			
Line 1	3.244e4	3.424e4	-5.26%
Line 2	3.244e4	3.429e4	-5.40%
Line 3	3.412e4	3.308e4	3.14%
Line 4	3.415e4	3.310e4	3.17%

Table 2 Bridge weight as 900 kg and wind direction **90** deg

	With bridge	Without bridge	Change
Natural period float	~29s	~29s	0
Equilibrium position (m)	(0.318,0.742,-0.035)	(0.294,0.144,-0.002)	(0.024, 0.598,-0.033)
Mooring Line Force (N)			
Line 1	3.84e4	3.552e4	8.11%
Line 2	3.177e4	3.437e4	-7.56%
Line 3	3.494e4	3.318e4	5.30%
Line 4	3.106e4	3.235e4	-3.99%

Table 3 Bridge weight as 900 kg and wind direction **45** deg

	With bridge	Without bridge	Change
Natural period float	~29s	~29s	0
Equilibrium position (m)	(0.642,0.432,-0.034)	(0.394,0.11,-0.002)	(0.248, 0.322,-0.032)
Mooring Line Force (N)			
Line 1	3.534e4	3.496e4	1.09%
Line 2	3.181e4	3.409e4	-6.69%
Line 3	3.479e4	3.328e4	4.54%
Line 4	3.231e4	3.265e4	-1.04%

- Wind in y-direction, the equilibrium position change in y-direction is approximate 0.6 m, corresponding to the largest one
- The changes of the mooring line forces due to the bridge effect are all within 10%
- The natural period of the floater does not change with or without bridge

References:

1 https://www.rina.org/en/media/CaseStudies/blue-growth-farm

2 Li, Liang, et al. "Analysis of the coupled dynamic response of an offshore floating multi-purpose platform for the blue economy." Ocean Engineering 217 (2020): 107943.

Dr Yan Gao
Research Associate
Department of Naval Architecture, Ocean & Marine Engineering | University of Strathclyde
HD2.16, Henry Dyer Building, 100 Montrose Street, Glasgow G4 0LZ, United Kingdom

An off-grid floating oscillating-water-column for powering oceanographic instruments

Charikleia L. G. Oikonomou, PhD, Research fellow, charikleiaoikonomou@tecnico.ulisboa.pt
Project supervisors: Prof Luís M. C. Gato, Dr Rui P. F. Gomes
IDMEC, Instituto Superior Técnico (IST), Universidade de Lisboa, Av. Rovisco Pais 1, 1049-001, Lisbon, Portugal

1. Introduction

Oceanographic monitoring systems (e.g. Acoustic Doppler Current Profilers (ADCPs), wave and current measurement buoys, Conductivity, Temperature, and Depths sensors (CTDs)) are designed to operate relying on a combination of renewable energy and energy storage systems. A common solution for powering these systems is a solar photovoltaic (PV) module with battery storage. The downside of using a solar PV is that due to the diurnal nature of the photovoltaic resource, a battery bank with a large storage capacity must be used, so that it allows the system to run autonomously for a sufficient amount of time. Therefore, a small wave energy converter or a hybrid wave-solar converter could present a more reliable solution [1,2].

Aim of the project: To evaluate the potential of an adapted floating oscillating-water-column wave energy converter for powering oceanographic equipment through experimental modelling.

2. The adapted spar-buoy OWC

The **spar-buoy Oscillating-Water-Column (OWC)** [3] consists of a partially submerged floater connected to a hollow spar tube which is open to the sea at its submerged bottom. An air chamber is contained above a water column inside the spar tube which is connected to the atmosphere via an air turbine. The incoming waves cause relative motion between the buoy and the OWC which results in compression and expansion of the air inside the air chamber and drives the air turbine connected to an electrical generator.

The adapted spar-buoy OWC design considered in this study was developed in the frame of the WAVEBUOY FCT project [4]. The geometry is similar to the one optimised by Gomes et al. [5], but its dimensions are different (Fig. 1). Due to the limited buoy size, its heave natural period is much lower than the typical wave period, and as a result the system is less efficient than the large buoys presented in Ref. [5]. This spar-buoy OWC is equipped with a biradial turbine which is an impulse-type air turbine, capable of operating close to its peak efficiency for a wider range of flow rates [4,6].

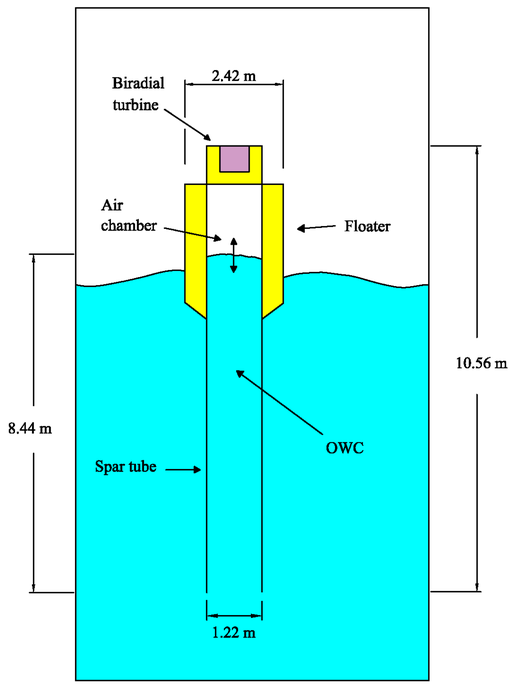

Fig. 1: Cross-section of the adapter spar-buoy OWC developed by Instituto Superior Técnico (IST), with full-scale dimensions.

3. Experimental set-up

- The **1:10th buoy model** was built from steel plate and Froude scaling criterion was adopted.
- The experiments were conducted in a wave channel at Laboratório Nacional de Engenharia Civil (LNEC) in Lisbon, Portugal. (Width = 2.96 m, length = 58.58 m, and water depth = 2 m).
- The facility is equipped with a piston-type wave maker and an absorbing structure for wave dissipation.
- The damping effect of the air turbine was replicated by an orifice plate mounted on top of the buoy.
- The six Degree-of-Freedom motion of the buoy was captured with the aid of an infrared camera.
- Six conductive wave gauges were deployed in various positions along the channel. A water level gauge was placed inside the buoy to measure the relative motion between the buoy and the OWC.
- Station-keeping was ensured by connecting the buoy to the channel walls with four equidistant nylon ropes (simplified mooring system).
- Fast-response differential pressure sensors were used to measure the air chamber pressure fluctuation which was necessary for determining the pneumatic power captured by the device.

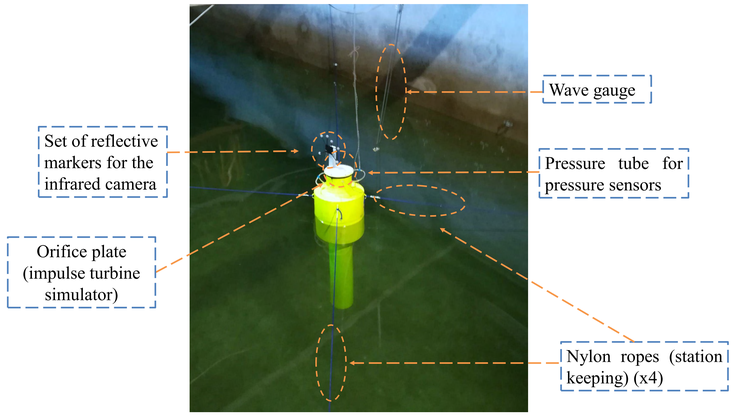

Fig. 2: The 1:10th spar-buoy OWC model with the installed equipment.

4. Results and discussion

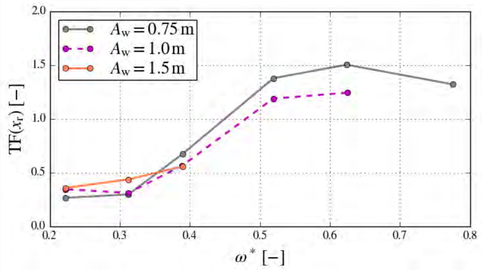

Fig. 3: Regular-wave transfer function of the relative motion between the buoy and the OWC against the dimensionless wave frequency for three wave amplitudes (full-scale).

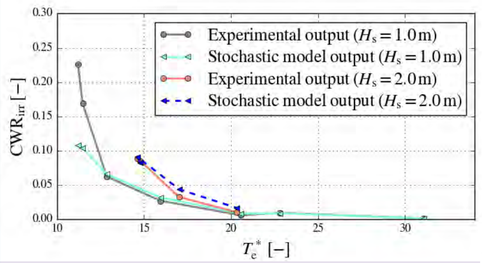

Fig. 4: Irregular-wave dimensionless capture width ratio against the dimensionless energy period for two significant wave heights (full-scale). The results also include output obtained from stochastic model analysis using experimental regular-wave data.

Tests were undertaken under regular and irregular wave conditions. Fig. 3 presents the transfer function of the relative motion between the buoy and the OWC (x_r) (which is equal to the amplitude of x_r divided by the measured wave amplitude A_w ,(as a function of the dimensionless wave frequency $\omega^*\left(\omega^* = {}^{\omega}/_{\sqrt{g/d}}\right)$ (where g is the acceleration due to gravity and d is the buoy diameter). Higher wave amplitudes A_w resulted in lower values of the relative motion transfer function. This is related to damping from viscous fluid effects, since higher waves introduce higher viscous losses to the spar-buoy OWC dynamics [7,8]. Fig. 4 concerns the irregular wave tests, and presents the Capture Width Ratio (CWR) against the dimensionless energy period T_e^* $\left(T_e^* = T_e/\sqrt{d/g}\right)$ for two significant wave heights H_s. The irregular wave tests were undertaken to validate the output from a non-linear stochastic formulation [9] which predicts irregular wave quantities based on regular-wave data. The overall good agreement between the experimental irregular wave results and those obtained from the stochastic model using experimental regular wave data encouraged the power matrix generation.

The spectral density of the Bretchneider spectrum is given by (SI units):

$$S(\omega) = \frac{5}{16}\frac{H_s^2\omega_p^4}{\omega^5}\exp\left(-\frac{5}{4}\left(\frac{\omega_p}{\omega}\right)^4\right)$$

where ω_p is the peak frequency. A location off the Outer Hebrides (Scotland) was selected, to evaluate the performance of the device. The probability of occurrence of each sea state is depicted in Fig. 5(a), based on hindcast data. The power available to the turbine $\bar{P}_{t,irr}$ in its annual-averaged form was determined by

$$\bar{P}_{ann,t,irr} = \sum_{i=1}^{N} F_i \bar{P}_{t,irr,i}$$

where F_i is the probability of occurrence of each sea state. According to Fig. 5(b), the annual-averaged power available to the turbine for this location was estimated to be approximately 1.7 kW. Considering 60% efficiency for the turbine and generator, the studied device with the selected power-take-off characteristics will meet the energetic needs of oceanographic instruments including ADCPs (typical requirement 20-500 W).

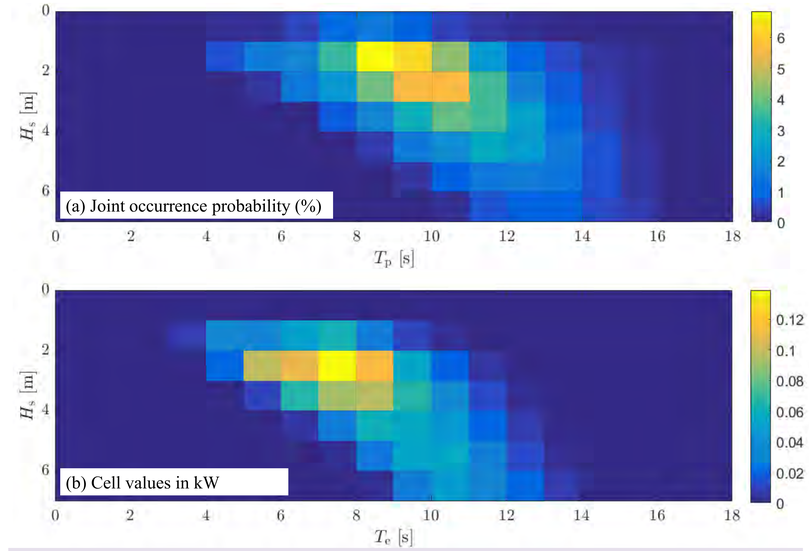

Fig. 5: Joint occurrence probability for H_s, T_p for the Outer Hebrides (WAVEWATCH III, 1979-2009) (a) and disaggregation table of the annual-averaged power per sea-state for the studied location ($T_e \cong 0.86T_p$) (b).

5. Conclusions

This work dealt with the experimental modelling of a floating OWC whose dimensions are relatively small compared to typical open sea wavelengths. The main conclusions can be summarised as:

1. Non-linear effects were apparent around the natural frequency, linked to the viscous damping.
2. There was good agreement between the irregular wave results and the stochastic modelling results.
3. For a wave climate off the Outer Hebrides, the power available to the turbine is sufficient for the supply of oceanographic instruments.

Acknowledgements

This work was supported by the Portuguese Foundation for Science and Technology (FCT) through IDMEC, under LAETA, project UIDB/50022/2020. Mr Juan Portillo (IST) assisted with the experimental set-up. Prof J. C. C. Henriques (IST) designed the 2.42 m diameter buoy and Mr D. Neves Ferreira (IST) designed and manufactured the buoy model. The experimental data were acquired with a code written by Prof. J. C. C. Henriques. Dr Juana Fortes (LNEC) allowed access to the facility.

References

[1] J. C. C. Henriques, J. C. C. Portillo, L. M. C. Gato, R. P. F. Gomes, D. N. Ferreira, A. F. O. Falcão, Design of oscillating-water-column wave energy converters with an application to self-powered sensor buoys, Energy 112 (2016) 852–867. doi:10.1016/j.energy.2016.06.054.
[2] C. L. G. Oikonomou, R. P. F. Gomes, L. M. C. Gato, A. F. O. Falcão, Preliminary experimental results of a 1: 10th scale model of a spar-buoy OWC for oceanographic purposes, in Developments in Renewable Energies Offshore: Proc. of the 4th International Conference on Renewable Energies Offshore (RENEW 2020, 12-15 October 2020, Lisbon, Portugal).
[3] A. F. O. Falcão, J. C. C. Henriques, J. J. Cândido, Dynamics and optimization of the OWC spar buoy wave energy converter, Ren. Energy 48 (2012) 369–381. doi:10.1016/j.renene.2012.05.009.
[4] J. C. C. Henriques, R. A. B. C. Crisóstomo, D. Neves Ferreira, L. M. C. Gato, R. P. F. Gomes, WAVEBUOY Deliverable 2 - Design of an OWC spar buoy for oceanographic purposes, Tech. rep., IDMEC internal report (2019).
[5] R. P. F. Gomes, J. C. C. Henriques, L. M. C. Gato, A. F. O. Falcão, Hydrodynamic optimization of an axisymmetric floating oscillating water column for wave energy conversion, Ren. Energy 44 (2012) 328–339. doi:10.1016/j.renene.2012.01.105.
[6] A. A. D. Carrelhas, L. M. C. Gato, J. C. C. Henriques, A. F. O. Falcão, J. Varandas, Test results of a 30kW self-rectifying biradial air turbine-generator prototype, Ren. and Sustain. En. Rev. 109 (2019) 187–198. doi:10.1016/j.rser.2019.04.008.
[7] C. L. G. Oikonomou, R. P. F. Gomes, L. M. C. Gato, A. F. O. Falcão, On the dynamics of an array of spar-buoy oscillating water column devices with inter-body mooring connections, Ren. Energy 148 (2020) 309–325. doi:10.1016/j.renene.2019.11.097.
[8] R. P. F. Gomes, J. C. C. Henriques, L. M. C. Gato, A. F. O. Falcão, Wave power extraction of a heaving floating oscillating water column in a wave channel, Ren. Energy 99 (2016) 1262–1275. doi:10.1016/j.renene.2016.08.012.
[9] C. L. G. Oikonomou, R. P. F. Gomes, L. M. C. Gato, Unveiling the potential of using a spar-buoy oscillating-water-column wave energy converter for low-power stand-alone applications.

Supergen Offshore Renewable Energy
Third Annual Assembly
Offshore Renewable Energy & the Road to Net Zero
Online
18 - 22 Jan 2021

Early Career Research Network

Dr Liang Yang
Lecturer in Marine renewable energy systems

Hydrodynamic performance of submerged hydrofoils subjects to coupled pitch and heave motion

Flow passing a foil object will produce lift and drag forces, as well as vortex street BvK. With right parameters, a periodic motion of an object in fluids generates thrust rather than drag. The hydrofoil motion with pitch and heave motion has been investigated using in-house CFD code. Different oscillation parameters of a NACA0012 hydrofoil were studied to optimise the performance of the thrust generation.

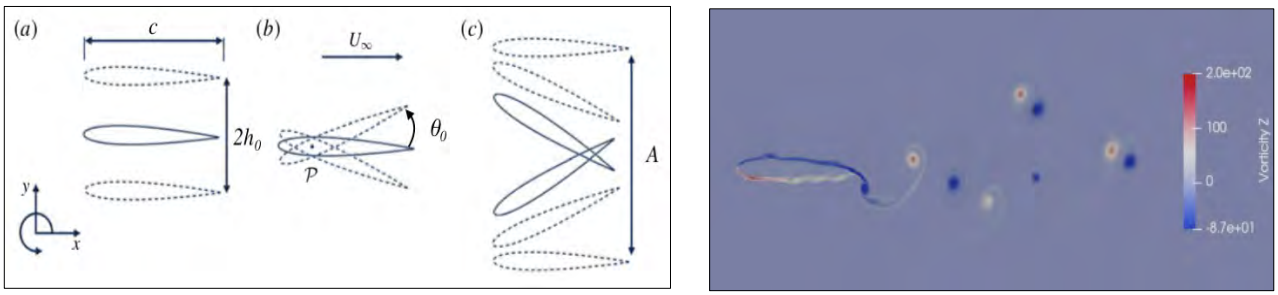

Flapping foil motion: a) pure pitch, b) pure heave, c) coupled pitch and heave

Conclusions

- Lift and drag coefficients were validated with the literature with different AOA under different Reynolds number
- Thrust coefficient were tested under different Strouhal number and validated
- Free moving case were tested, same computational costs as fixed case
- Experimental work will be carried out

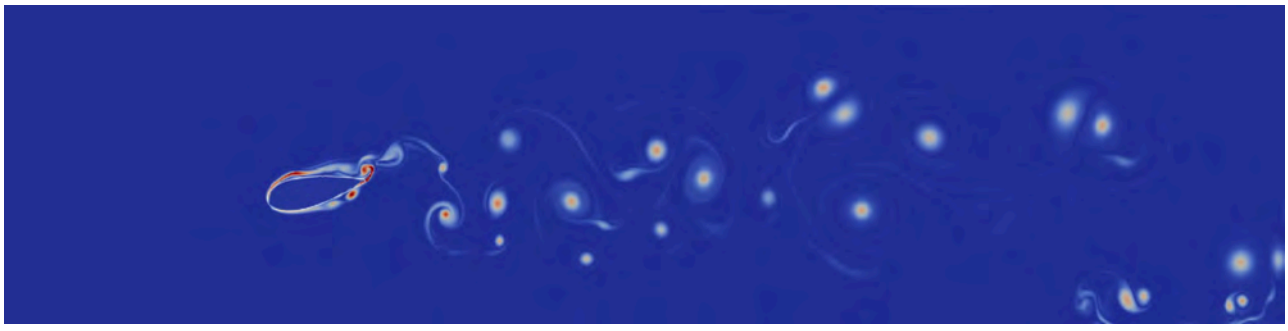

www.cranfield.ac.uk

E: liang.yang@cranfield.ac.uk
W: cranfield.ac.uk/people/dr-liang-yang-23276693

MODELING VALIDATION OF HINGED-RAFT WAVE ENERGY CONVERTER USING WEC-SIM

Siya Jin, Deborah Greaves
School of Engineering, Computing and Mathematics, University of Plymouth

Engineering and Physical Sciences Research Council

Supergen Offshore Renewable Energy

ABSTRACT

This study evaluates the feasbility of using the free open-source modelling toolox Wave Energy ConverterSIMulator (WEC-Sim) to model a hinged-raft wave energy converter (WEC). A generic hinged-raft WEC is selected and studied. The results obtained from WEC-Sim and the published analytical modelings are compared. The results show that WEC-Sim can model the performance of hinged-raft effectively, with the scripts under function 'Read_AQWA' modified.

GENERIC HINGED-RAFT WEC

A generic hinged-raft WEC, which has been studied by Newman (1), Sun et at. (2)and Zheng et at. (3) is selected and studied. The front and back raft are cuboid and symmetrical along the hinge point. The detailed geometric parameters are shown in the figure given in below.

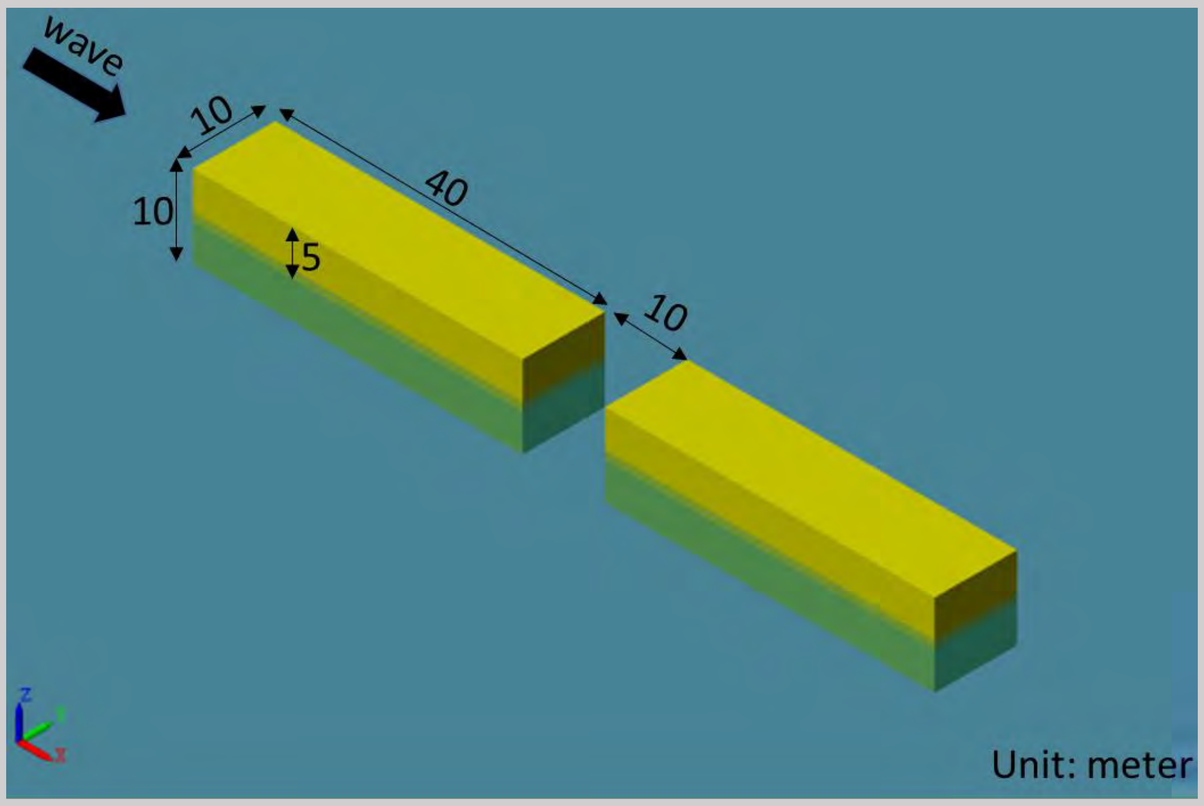

PROBLEMS IN WEC-SIM

The function 'Read AQWA' in WEC-Sim is found to have following problems in reading hydrodynamic coefficients generated from AQWA:

- ***Phase of the excitation force***
- ***Radiation damping and added mass matrix***

RESULTS

The comparison is conducted and shown in figures in below. The results are obtained from:

- WEC-Sim with original function 'Read_AQWA'; with modified function considering excitation phase shift (WEC-Sim correction1); with modified function considering both excitation phase shift and radiation damping & added mass matrix correction (WEC-Sim correction2)
- Self-edited code based on Lagrange multiplier technique (Jin) and the published papers by Newman using mode expansion technique(Newman) and Zheng et at. using Lagrange multiplier technique (Zheng et al.)

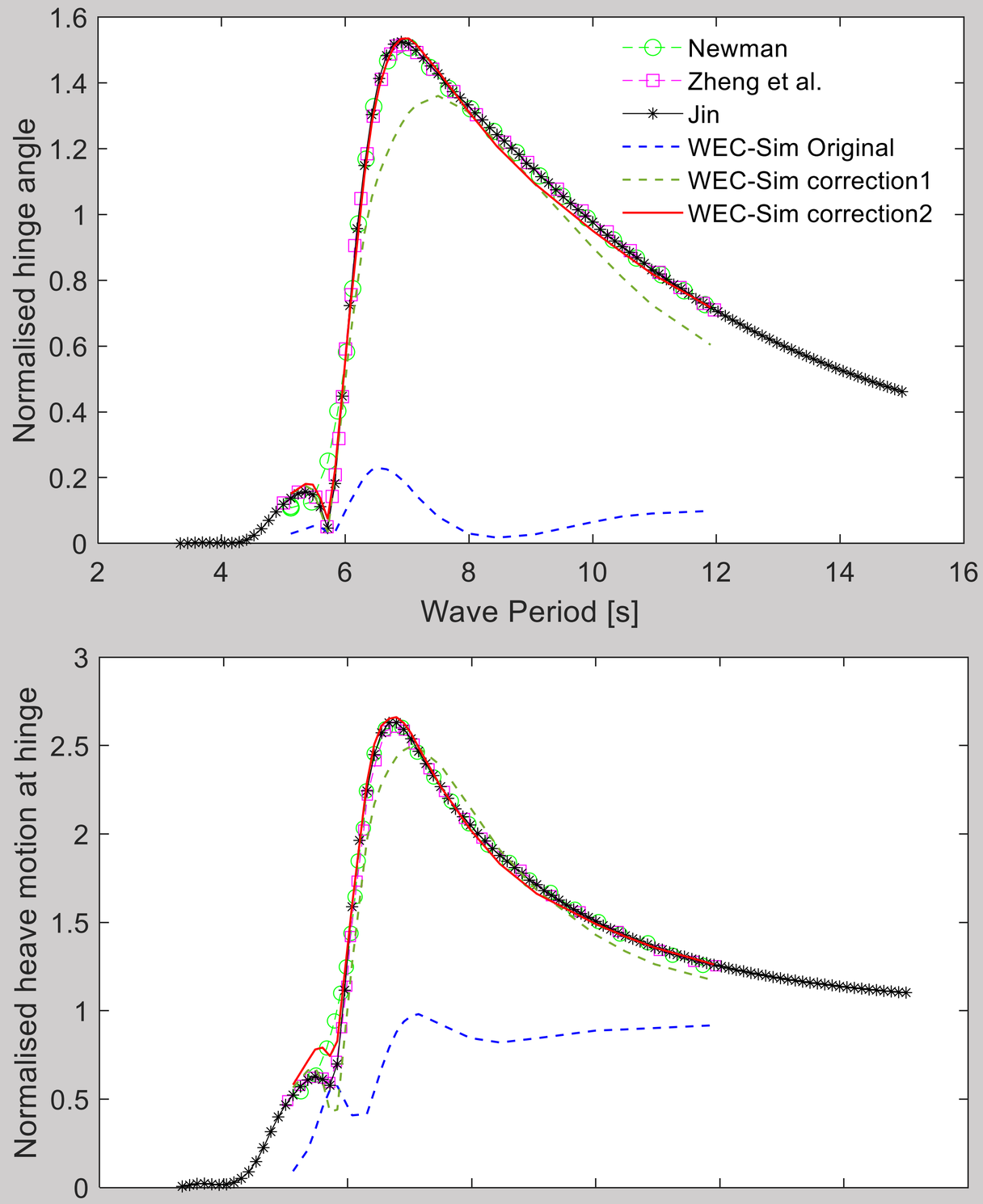

DISCUSSIONS & CONCLUSION

This work evaluates the effectiveness of WEC-Sim in modeling hinged-raft WEC. It can be found that to effectively model hinged-raft WEC using WEC-Sim, the function 'Read_AQWA' needs to be modified to consider excitation force phase shift; to correct the radiation damping and added mass matrix

Reference : (1) Newman, J.N., 1994. Wave effects on deformable bodies. Applied Ocean Research 16, 47–59.
(2) Sun, L., Taylor, R., Eatock, Choo, Y.S., 2011. Responses of interconnected floating bodies. The IES Journal Part A: Civil and Structural Engineering 4 (3), 143–156.
(3) Zheng, S.M., Zhang, Y.H., Zhang, Y.L. and Sheng, W.A., 2015. Numerical study on the dynamics of a two-raft wave energy conversion device. Journal of Fluids and Structures, 58, pp.271-290.

Climate change impact on structural performance of offshore wind turbines

David Wilkie (david.wilkie.15@ucl.ac.uk) Dr Carmine Galasso (c.galasso@ucl.ac.uk)

1) Motivation

The assessment of offshore wind turbines (OWTs) is currently based on **fixed assumptions about the future climate**. However, any changes in the wind climate may effect both:

- Energy produced by the OWT, as this depends on the mean wind speed (V_w) as shown Figure 1 (left)).
- Structural loading experienced by the OWT over it's life.

However, predicted changes in environmental conditions are not homogeneous across European water, Figure 1 (right) from [1], and studies have provided varying estimates of the future wind climate.

This work therefore **quantifies the impact of changing wind climate on OWT energy production and structural fatigue damage using a parametric approach**.

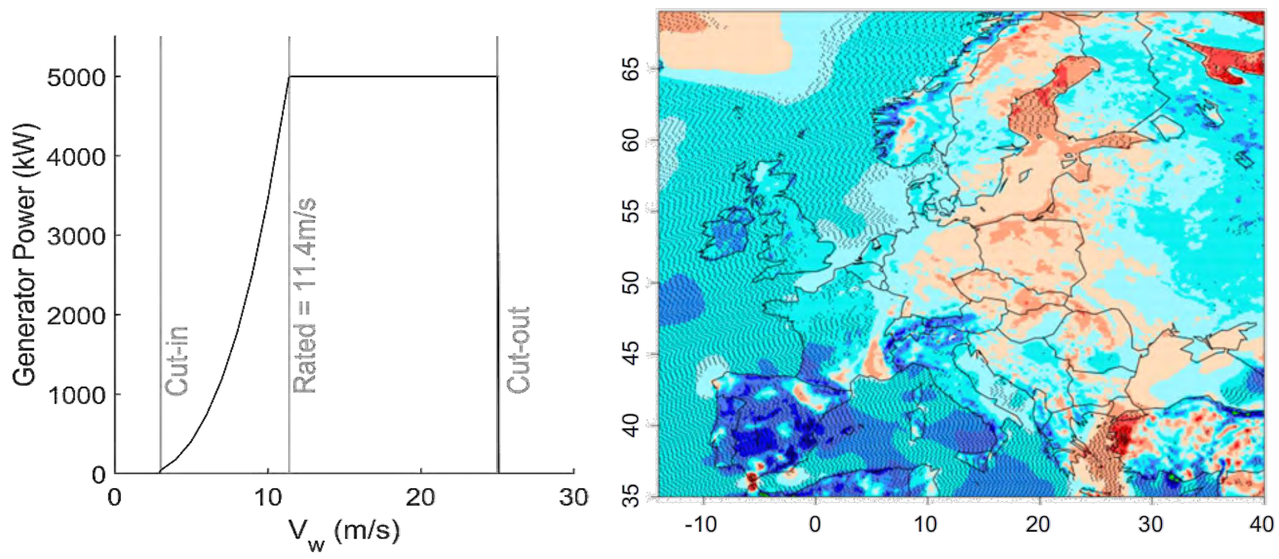

Figure 1 – OWT performance curve [2] (left), changes in wind speed as a result of climate change red=increase, blue=decrease (right)

2) Model

Impact of climate change
Through scale and shape parameter of mean wind speed

The scale and shape parameter of the V_w distribution affect the behaviour of the OWT in non-linear manner.

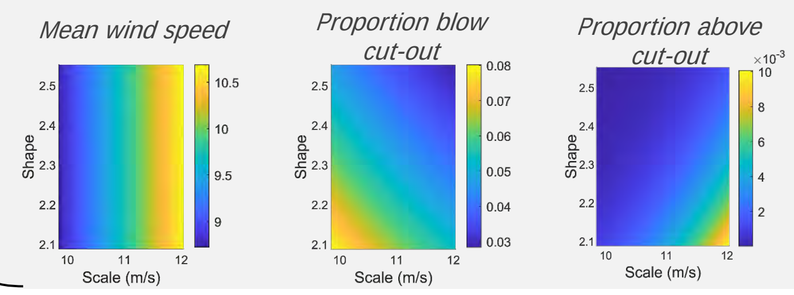

Other environmental condition
Using measured correlations

The scale and shape of the V_w distribution also influence the distribution of other environmental parameters (such as wave height) through correlation.

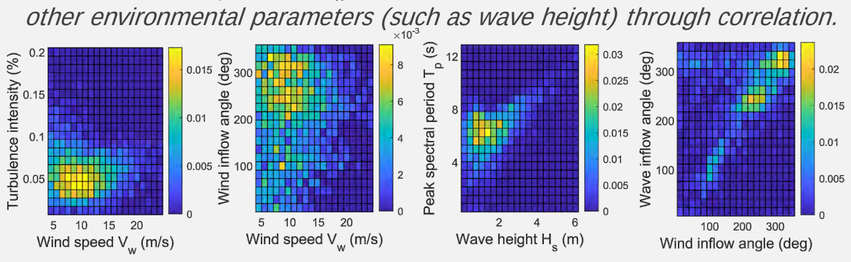

A set of 45 representative V_w scale and shape parameters were selected, and the resulting distribution of other environmental parameters were then generated for each.

Structural response
Using time-history analysis

Machine learning
Fit Gaussian process meta-model to the structural analysis.

A Gaussian process model allowed fatigue damage for each combination of V_w scale and shape parameters to be calculated in a computationally efficient manner.

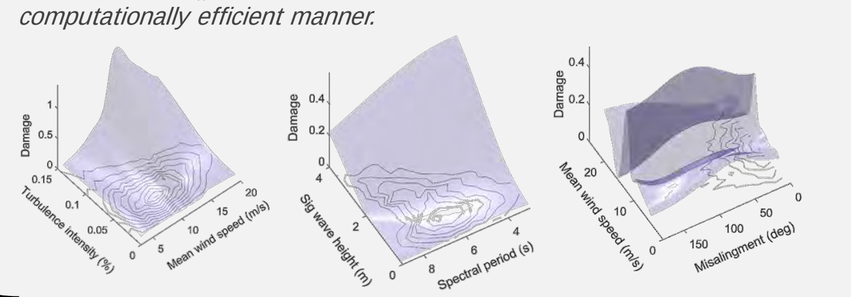

Calculate performance metrics
For structure and power production

3) Impact on structural performance metrics

Fatigue damage and probability of structural failure (P_f) were sensitive to changes in the scale and shape of the V_w distribution.

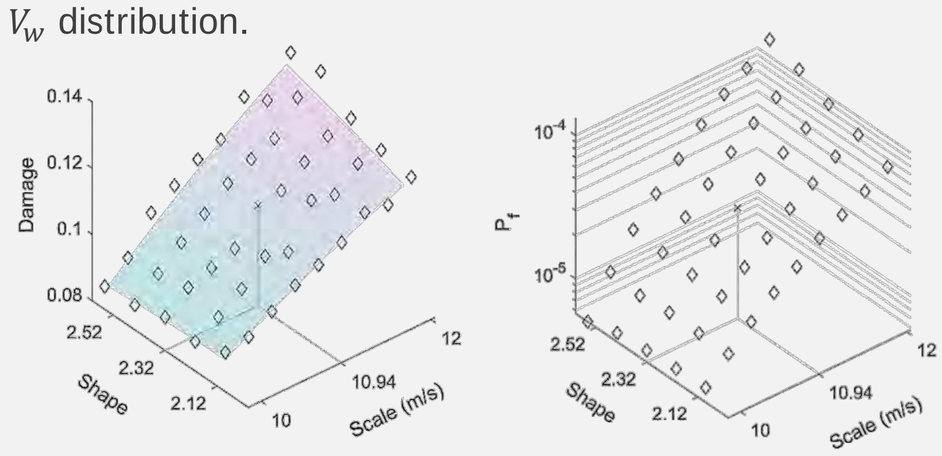

Climate change had little impact on the expected annual losses due to high failure rate of the equipment components (such as the generator and rotor bearings).

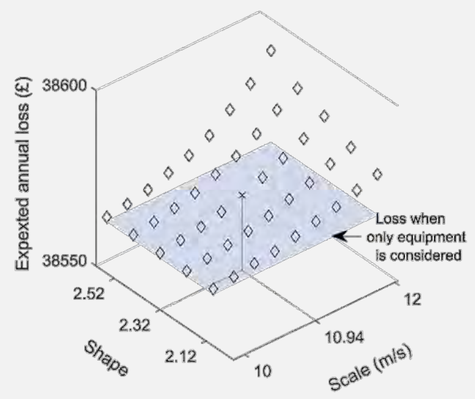

4) Comparison

The different performance metrics were compared for the scale (λ) and shape (k) parameters. Indicating high sensitivity in the probability structural failure and revenue loss.

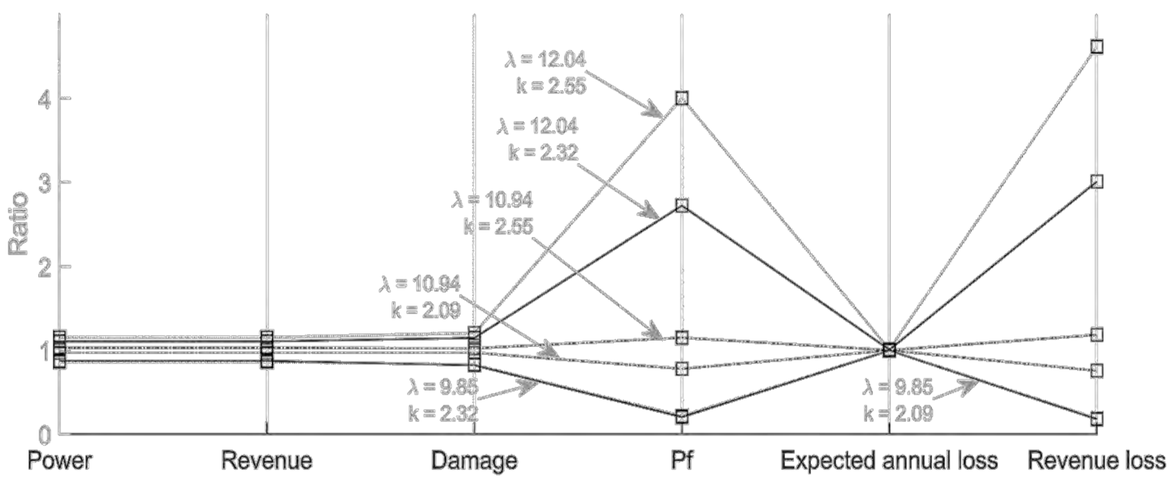

5) Conclusion

- The wind turbine probability of **fatigue failure and revenue loss resulting from failure of the structure were found to be very sensitive** to wind speed parameter changes.
- These parameters depend on the fatigue damage which is sensitive to changes in wind speed (to the power of 5-7). More so than power production (to the power of 3).
- Therefore **small changes in the wind speed may have greater impact on OWT structural performance metrics**.
- Caveat – climate changes will occur over the OWF life, whereas this study neglects this time-dependency.

References
[1] Tobin I et al. Climate change impacts on the power generation potential of a European mid-century wind farms scenario. Environ. Res. Lett [2016]. doi:10.1088/1748-9326/11/3/034013.
[2] Jonkman J et al. Definition of a 5MW reference wind turbine for offshore system development. NREL [2009].

Capacity of Driven Piles in Chalk

Fabian Schranz & Róisín M. Buckley
Department of Engineering Science, University of Oxford
Fabian.Schranz@eng.ox.ac.uk

ALPACA: Axial-Lateral Pile Analysis for Chalk Applying multi-scale field and laboratory testing (EPSRC Grant EP/P033091/1)

R.J. Jardine (PI) and S. Kontoe, Imperial College London; B.W. Byrne and R.A. McAdam, Oxford University

Problem:

- Many construction sites in chalk
- Chalk is a low-density, porous weak carbonate rock
- High uncertainty for designers
- Few field pile test results for axial and lateral capacity

Aims of ALPACA and ALPACA+:

- Axial and lateral pile tests on 40 piles driven in chalk
- Parallel laboratory research, in situ testing and analysis
- New design guidance for tubular piles in chalk

Chalk Across Northern Europe

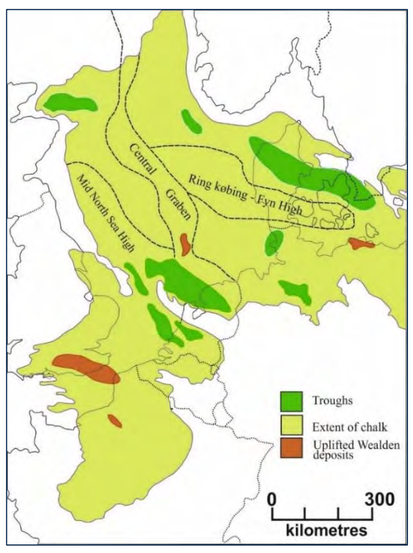

Chalk deposits are found over large areas across northern Europe. Most off-shore wind farms are founded on chalk.

Test Site (St. Nicholas-at-Wade)

14 by 0.5 m diameter piles were driven in a chalk test site in November 2017. They were tested over the June to October 2018 summer period.

Test Types

Axial static tension and one-way cyclic tests

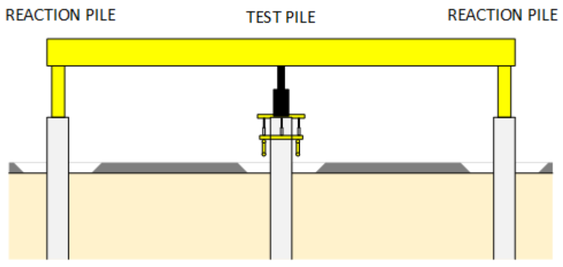

Axial static compression and two-way cyclic tests

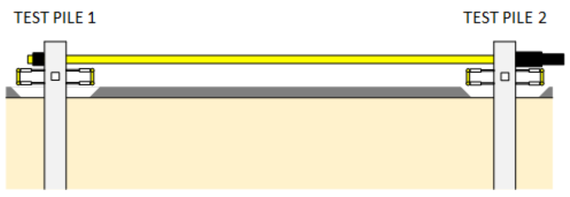

Lateral static and cyclic tests

Example Test Results (ALPACA programme)

Fibre optic strains along pile monitored during driving blows

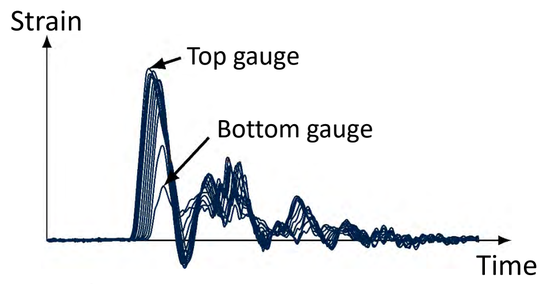

Typical axial load vs. displacement result

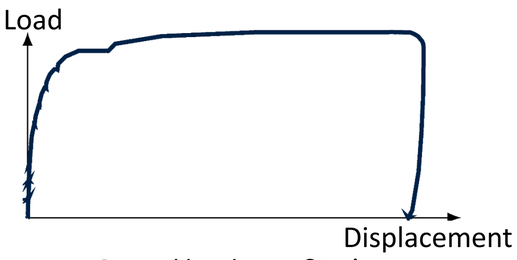

Typical distribution of strain during lateral test

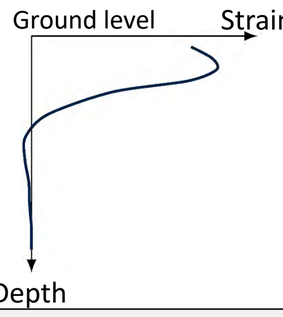

ALPACA+

- Extension to main programme
- Investigation of pile diameter and wall thickness ratio
- New large piles installed in November 2020
- Tests to be completed in mid-2021